2009

Real Time Physical Analysis of Consolidation Process for Low Pressure Gas Dynamic Spray

Mark Lubrick
University of Windsor

Real Time Physical Analysis of Consolidation Process for Low Pressure Gas Dynamic Spray

By
Mark Lubrick

A Thesis
Submitted to the Faculty of Graduate Studies
through Physics
in Partial Fulfillment of the Requirements for
the Degree of Master of Science at the
University of Windsor

Windsor, Ontario, Canada
2009

Declaration of Co-Authorship / Previous Publication

I. Co-Authorship Declaration

I hereby declare that this thesis incorporates material that is result of joint research, as follows:

This thesis incorporates the outcome of a joint research undertaken in collaboration with Volf Leshchynsky and Fedor Severin under the supervision of Professor Roman Maev. The collaboration is covered in Chapter 4 of the thesis. In all cases, the key ideas, primary contributions, experimental designs, data analysis and interpretation, were performed by the author, and the contribution of co-authors was primarily through the provision of advice and guidance. The exception is Dr Leshchynsky who also assisted with some of the writing, especially relating to the introductory chapters that discussed historical developments.

This thesis also incorporates the outcome of a joint research undertaken in collaboration with Volf Leshchynsky and Serge Titov under the supervision of Professor Roman Maev. The collaboration is covered in Chapter 6 of the thesis. In all cases, the key ideas, primary contributions, experimental designs, data analysis and interpretation, were performed by the author, and the contribution of co-authors was primarily through the provision of experimental hardware and advice.

I am aware of the University of Windsor Senate Policy on Authorship and I certify that I have properly acknowledged the contribution of other researchers to my thesis, and have obtained written permission from each of the co-author(s) to include the above material(s) in my thesis.

I certify that, with the above qualification, this thesis, and the research to which it refers, is the product of my own work.

II. Declaration of Previous Publication

This thesis includes 1 original papers that have been previously published/submitted for publication in peer reviewed journals, as follows:

Thesis Chapter	Publication title/full citation	Publication status*
Chapter 4	Young's modulus of low-pressure cold sprayed composites: an analysis based on a minimum contact area model, M. Lubrick, R.Gr. Maev, F Severin, V Leshchynsky. J Mater Sci (2008) 43:4953-4961.	*Published*

I certify that I have obtained a written permission from the copyright owner(s) to include the above published material(s) in my thesis. I certify that the above material

describes work completed during my registration as graduate student at the University of Windsor.

I declare that, to the best of my knowledge, my thesis does not infringe upon anyone's copyright nor violate any proprietary rights and that any ideas, techniques, quotations, or any other material from the work of other people included in my thesis, published or otherwise, are fully acknowledged in accordance with the standard referencing practices. Furthermore, to the extent that I have included copyrighted material that surpasses the bounds of fair dealing within the meaning of the Canada Copyright Act, I certify that I have obtained a written permission from the copyright owner(s) to include such material(s) in my thesis.

I declare that this is a true copy of my thesis, including any final revisions, as approved by my thesis committee and the Graduate Studies office, and that this thesis has not been submitted for a higher degree to any other University or Institution.

Abstract

The gas dynamic spray process is studied via acoustic methods with the main focus being on developing an online system to monitor the process as it occurs. Elastic modulus measurements of the coatings are determined from the sound velocity and porosity. The resulting data is than compared against a minimum contact area model that is developed to describe the bonds that are formed between particles. The results show a good fit to the theoretical considerations of the model. Different transducer designs are considered leading to the use of a multi-element flat transducer for the online monitoring. Online measurements show that the build-up of the coating can be directly seen as well as accurate profiles of the coating created. Finally the online results are shown to be able to accurately predict thickness measurements of the coating acoustically.

Table of Contents

List of Tables

List of Figures

List of Abbreviations

GDS –	Gas Dynamic Spray
LPGDS –	Low Pressure Gas Dynamic Spray
HPGDS –	High Pressure Gas Dynamic Spray
TEM -	Transmission Electron Microscopy
SEM –	Scanning Electron Microscope
MMCs -	Metal Matrix Composites
Al –	Aluminum
Ni –	Nickel
Cu –	Copper
Ti –	Titanium
TiC –	Titanium Carbide
SiC –	Silicon Carbide
MCA –	Minimum Contact Area
NMCA –	Normalized Minimum Contact Area
SAM -	Scanning Acoustic Microscope
ASB -	Adiabatic Shear Bands

Chapter 1

Introduction

1 Purpose

The gas dynamic spray (GDS) process or "cold spray" is a burgeoning coating technology that is still mostly in the development stage. It has huge potential and is already in use in many different industrial sectors; however, to reach its full potential it will need to be fully understood and characterized, which presently has not been done. The use of ultrasonic techniques is a well-established and understood technology. A common application of ultrasonics is for the use of non-destructive testing. With the proper considerations, it is possible to characterize the samples being studied and even draw conclusions about whatever process is being studied. In fact, it is already well established that the spot welding process may be studied and monitored during the actual welding process [1]. These considerations led to the idea that perhaps the GDS process could be studied and become better understood with the use of ultrasonic techniques. Thus the purpose of this work was to attempt to study the GDS process and characterize its properties based on ultrasonic properties, with the main focus being on developing a system to monitor the process online (as it happens).

Now that a goal is in mind, it is important to expand upon any vague points and to establish how best this task can be undertaken. The easiest way to do this is to consider each point of the purpose on its own. The rather simply stated first goal was to study the GDS process with ultrasonics. While a detailed explanation of how ultrasonics works is left to chapter 3 for now it is suffice to say that many types of data and even images may be acquired through processing of the acoustic signal. While the basic purpose of this

study would be to become familiar with both GDS and ultrasonics and the interactions therein, it is possible to make qualitative assessments with very little experience. Figure 1.1 shows a typical C scan (more on this later) which is a cross section of the samples. It is clearly seen that some regions are lighter and some much darker which leads to a simple estimate that the lighter regions are not bonded as well (more reflection at this point). These types of qualitative assessment have limited usefulness however since it is impossible to estimate how much "better" one region is to another especially if comparing more than one sample.

Those considerations lead to the second aspect of the purpose, namely characterizing the properties of the GDS process based on ultrasonic properties. This is meant to allow for the determination of quantitative data as well. The output of the ultrasonic signals can be made as quantitative data allowing for the comparison between different samples however, these comparisons are only useful if they correspond to some type of change within the coating. Thus, it is necessary to establish relations between the quantitative ultrasonic properties and structural properties of the coating. In order to do this it is necessary to establish models that describe how a measurable ultrasonic property

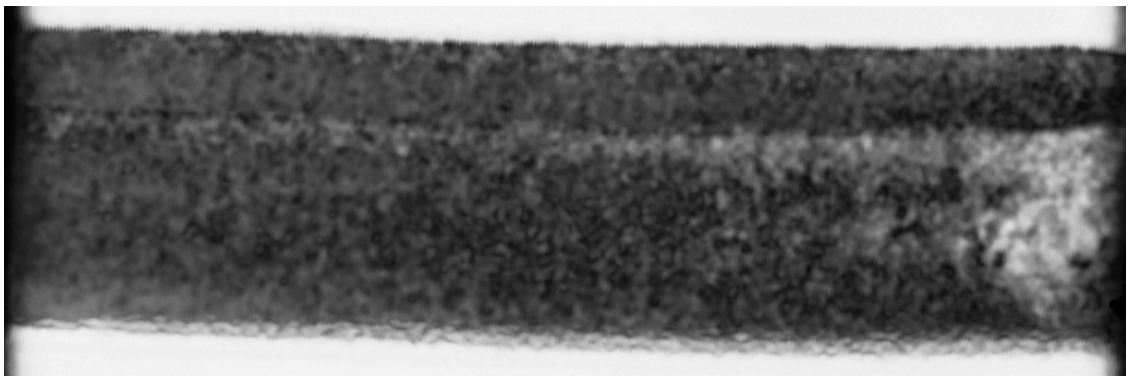

Figure 1.1 Example of C scan image.

is related to some structural property and how they change in relation to each other. This is the basis for establishing non-destructive predictions of the coating properties

Finally, the last purpose of this thesis is the development of an ultrasonic online monitoring process for GDS. Simply put this part uses ultrasonic equipment to create a method for monitoring the GDS process as it actually occurs. The hope is that in the future this may be used to help characterize how the GDS process works as well as using previously developed and future models to asses coating properties during the bonding process.

2 Gas Dynamic Spray

While an in-depth discussion of the GDS process is left to the next chapter, there are some important points to establish from the offset. One such thing is that this research was all conducted using a low-pressure GDS (LPGDS) machine as shown in figure 1.2 and developed by Centerline Limited [2]. In this set up, the gun is mounted on a robotic arm that can traverse within the chamber in the x y and z directions. The movement of the gun is controlled by preset programs that tell it when to spray and what directions to move, though the gun may also be removed and samples sprayed by hand. The gun may also spray at a range of temperatures and pressures from approximately 0-600^{o}c and 0-12 bar (though in this case the pressure was limited to 6 bar by the compressor available). Figure 1.3 also shows an example of some of the samples that are created using this technology. For the top row, the left sample is nickel and titanium carbide sprayed on aluminum, while the other two are aluminum and alumina composites sprayed on steel. From left to right the bottom row is copper and titanium carbide

Figure 1.2 Low-pressure gas dynamic spray unit developed by Centerline Limited [2] used to spray all samples.

sprayed on steel, two pure aluminum samples removed from substrate (steel), nickel on aluminum and finally aluminum and alumina composite on steel. As compared to LPGDS there is also high pressure GDS (HPGDS) that other researchers use. While each process is similar in many ways it is important to first consider the differences. Simply put the low-pressure case was used for these studies because as it stands it is more feasible for applications. The advantages high-pressure gains in density and strength of coating are more than outweighed by the lack of any type of portability and the higher costs associated. Through careful analysis of the process, coatings may be improved by many properties besides just the pressure/velocity of the airflow. Since the low pressure,

case is already highly portable and much lower cost these improvements to the coating quality currently make the low-pressure case much more viable for applications in this author's opinion.

The GDS process in general is still new and not well understood. In fact, while there are theories, it has not been conclusively shown as to how the exact process works. This is why it is so terribly important to study and attempt to characterize the process. This technology can only be improved through a deeper understanding of the physics behind how it works. It is especially important to begin to characterize the properties of

Figure 1.3 Examples of cold sprayed samples for study. (top- left to right nickel composite on aluminum, 2 aluminum composites on steel, bottom- left to right copper composite on steel, 2 pure aluminum, nickel composite on aluminum, aluminum composite on steel)

the coating itself. Being able to apply a coating is fine but if it does not meet the basic criteria required by the application (porosity, adhesion, etc) than it will be useless. To this author *et al* the most logical point to start at was a consideration of the actual physical geometry within the coating specifically porosity and the bonds within the coating. This was decided since these properties were believed to have a qualitative effect on most properties within the coating.

3 Ultrasonics

Again an in depth explanation of ultrasonics is left to chapter 3 however its worth mentioning here since it is such an integral part of the thesis. Currently other than works published by this author *et al* there appears to be no publications that use any ultrasonic technique to study the GDS process. This seems to add some significance to this and any future work made along these lines. Ultrasonics already has wide applications for use in non-destructive testing, thus it seems completely reasonable that similar considerations may be applied to the GDS process. Once appropriate models are developed it may be possible to test and determine properties of a coating non-destructively. This could be largely beneficial for any business applications as it would reduce costs and increase reliability. Perhaps even more importantly by using ultrasonics to monitor the process as it happens it should be possible to gain a deeper understanding of how it works and find ways to make improvements based on these finds. Lastly if the online monitoring can be regularly incorporated with the spraying apparatus this could allow for constant monitoring of the process as it happens leading to improved coatings and perhaps even some type of feed back system.

As will be expanded upon in chapter 3 ultrasonic studies can be conducted in two different modes, with a range of frequencies, can be used to image interior features of samples, and can even be used to monitor in real time. Finally figure 1.4 shows many of the types of transducers/machines that are used throughout this work.

4 Layout of the work

Before progressing into the work, it seems prudent to explain the basic layout of the thesis. The thesis was based on a manuscript type format so most of the chapters are self sufficient with their own bibliography. However, it is still imperative that the thesis has a general flow and continuousness towards a final goal. As stated above the final goal of this work is to establish a system to do ultrasonic online measurements of the GDS process. With that said, a more detailed explanation of the chapters within the thesis is given below.

Chapters 2 and 3 are meant to give a description of how the cold spray and ultrasonic processes work for readers who are unfamiliar with them. Chapter 4 is where the bulk of the work starts. It demonstrates some of the preliminary studies of the GDS process using ultrasonics and establishes some of the most important properties to consider (sound velocity, porosity, etc). This chapter also shows the model that was developed to help describe the types of bonds that are formed during the GDS process. In fact, this chapter is a very good demonstration of the way continued research should take place. First, the process was studied and based on the results characterization and models were

a

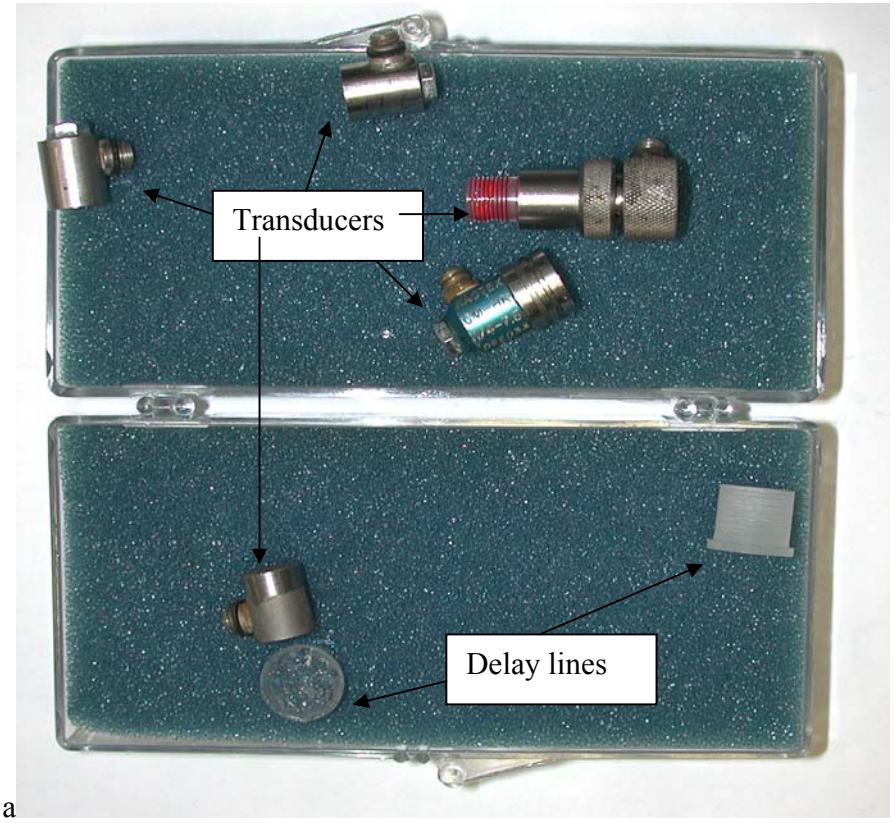

b

Figure 1.4 a-Flat transducers and delay lines, b-Scanning acoustic microscope (focused transducer).

developed. This type of research will need to be performed based on the results of the online analysis.

Chapter 5 focuses on the different types of transducers/machines used in ultrasonic techniques and how they can affect the results obtained. This chapter lays the framework for choosing what transducer to use for the online measurements as well as how to obtain and analyze the data required.

Chapter 6 than shows the development of the online ultrasonic measurements and the results obtained so far. Finally, chapter 7 gives a final discussion and points out what future work needs to be done.

References

1. A. Chertov, R. Maev, F Severin, Acoustic Microscopy of Internal Structure of Resistance Spot welds, IEEE Vol. 54 No. 8 August 2007 p. 1521-1529.

2. CenterLine (Windsor) Limited**,** http://www.cntrline.com, as on 16 June 2008.

Chapter 2

Introduction to Gas Dynamic Spray

1 Basics

Before getting into any details, it is important to try to prevent an area of potential confusion. As with many new processes Gas Dynamic Spray (GDS) has been referred to by many names, therefore for future clarification, it is important to note that GDS is also referred to as “cold spray”, “kinetic energy metallization, “kinetic spraying”, and “high velocity powder deposition” [1]. Furthermore, GDS is generally characterized as part of a larger category termed thermal spray techniques. These techniques are often used for sealing, welding, repairing, and coating various surfaces. Cold spray however, due to its unique properties, can do much more than just these basic functions (we will discuss this in more detail later).

When defining the GDS process it is often useful to start with some background knowledge of thermal spray techniques in general. In regular thermal spray processes, particles of a substance (most often metallic in nature) are superheated as they move through a tube. These molten particles are than accelerated towards the surface they are meant to cover (substrate) where they adhere. The principle idea behind cold spray is the same with some changes in the conditions. The cold spray process incorporates much higher velocities (approximately 500-900 m/s compared with 100-200 m/s) and much lower temperatures than normal thermal spray techniques (see figure 2.1). One of the main reasons the particles (typically around 10-50 microns) are still heated in cold spray is to ensure a higher acceleration for the particles is attainable. In fact, the gas cools

quickly in the nozzle and therefore the gas has little time to heat the particles and they remain at a much lower temperature than the carrier gas.

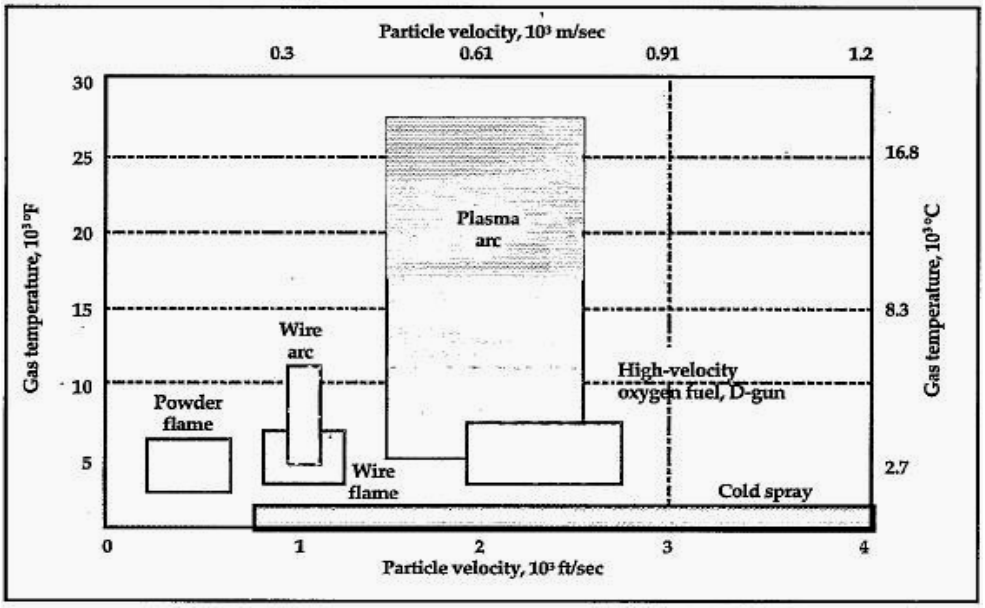

Figure 2.1 Plot comparing thermal spray processes based on particle temperature and particle velocity.

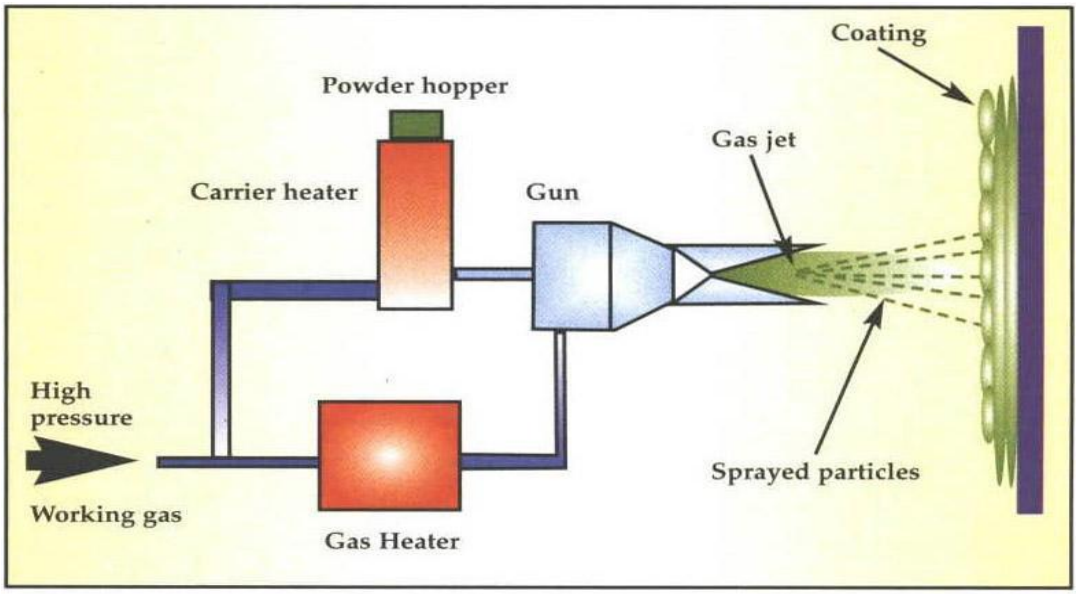

Figure 2.2 Layout of typical HPGDS.

2 Equipment

The GDS process itself can be split into two main types: high pressure and low pressure. While the main difference between the two is obvious from the name (pressure used) there is also another difference evident from figures 2.2 and 2.3, namely where the powder is injected into the carrier gas. To expand on this it is necessary to describe how the process works in general. High-pressure gas is accelerated (the velocity relies on the type of gas) through a heater and thus heats the gas [2]. An important thing to note is that the gas is always heated to a temperature less than the melting point of the powder. From there the gas enters the "gun" and this is where the two processes differ. For high pressure, GDS (HPGDS) the particles will be injected into the carrier gas within the gun. However, for low pressure GDS (LPGDS) the carrier gas passes through the convergent part of the nozzle to the divergent part and within this is where the particles are injected. In both cases saying the particles are injected may be a poor choice of words. In fact, the powders are fed by a powder hopper, but it is the negative pressure formed by the passage of the carrier gas that draws the particles into the stream. The accelerating gas

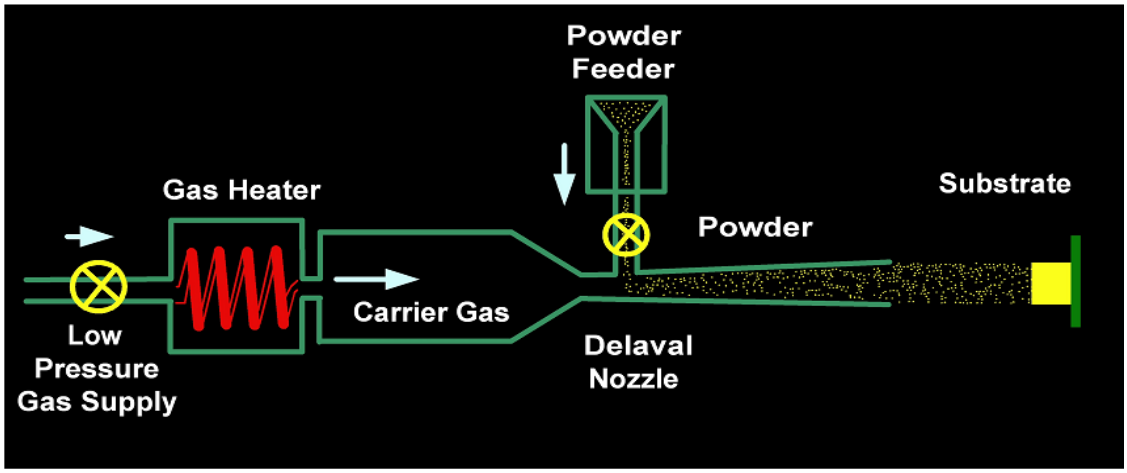

Figure 2.3 Layout of typical LPGDS.

causes the particles to be “swept along” at the high velocity of the gas. Again, for both processes the gas/particle mix exits out a diverging nozzle, this, due to the previously mentioned heating, allows for further acceleration of the particle. Finally, the particles come into collision with the substrate material.

Before progressing any further, it is important to mention that all research for this thesis was carried out using LPGDS technology. While both techniques have their advantages (HPGDS can potentially get higher density and strength of coatings), it is the opinion of this author that LPGDS has more potential now. Pressure is only one of the variables that affect the coating properties and may be overcome by changing other properties (powder size/geometry, type of carrier gas, powder concentration, temperature of particles and or substrate, etc). Thus, the potential benefits of HPGDS must be weighed against its faults. HPGDS requires very large facilities, generates a lot of noise and typically requires a long time to switch from one application to another. In fact, the machinery itself typically requires a large room to itself and even more room for generators. These disadvantages make it more difficult for industrial applications and virtually impossible for any purpose that requires mobility. LPGDS on the other hand is quieter, can switch between jobs extremely easily, and is a fraction of the size. In fact, there are LPGDS machines that can be easily rolled around and weigh as little as 100 pounds [6]. The portability is one of the most important aspects of this technology. It may easily be moved to whatever application for which it is required. This is extremely useful when compared with the high-pressure technology that requires parts to be brought to the facilities.

One last thing to discuss is the carrier gas. The carrier gas obviously has a large effect on the entire process and can significantly control the velocities obtainable. Air is the simplest and least expensive however, it also allows for the least speed. Nitrogen and helium are also commonly used though they do have their faults. While nitrogen leads to greater speeds than air and helium even more so they also have much higher costs (helium is more costly than nitrogen).

3 Bond Formation

So far, a large piece of the puzzle has been left out. GDS has been described as a coating process and in the last section, it left off at the point where the particles collide with the substrate. Now what? Obviously, for a coating process it means the particles adhere to the substrate, but how? The interesting thing is that this is not fully known. The exact bonding method is still being characterized for GDS (in fact this and future work was hoped to help characterize this) but there is some commonly accepted theories that are supported by data obtained from experiments and optical images (more on this latter). First, however it is important to start simple. When the particle collides with the substrate, 3 different things can occur depending on the kinetic energy (most importantly velocity) of the particle [2]. If the velocity is low enough the particle will simply reflect off the surface. If the velocity is increased, the particle will begin to damage (erode) the surface. However, once the velocity passes a certain critical value the particles will begin to form a layer on the substrate and on each other [2]. Figure 2.4 shows how this layer begins to form. At first, the substrate is likely to have contaminants on its surface, as the top picture shows the first particles will impinge off eroding or cleaning those

contaminants from the surface. The middle picture than shows that once the surface is clean if the particles have a high enough velocity they will begin to adhere to the surface. The bottom picture shows the final step where other particles collide with those already coated causing densification (particles are further deformed and fill gaps increasing density) and further build-up of coating.

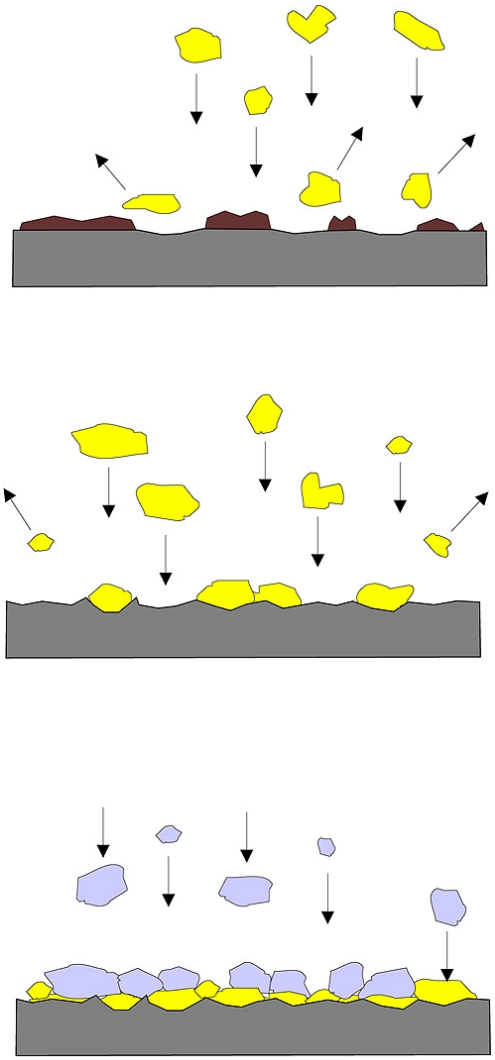

Figure 2.4 Coating formation top- surface cleaning, middle- coating forms, bottom- impinging particles cause densification of coating and continued build up.

The velocity at which the particles begin to form a layer is unique to each type of material sprayed (typical values are 500-900 m/s). There are two important things to note though. For one thing, the temperature of the particle and/or substrate also influences the bonding of particles to substrate and can diminish this critical velocity. Also within the particles being propelled by the carrier gas there will be a variety of particle velocities. Thus, not all particles will bond and in fact, those close but just under the critical velocity can damage those particles already bonded. Therefore it is important to adjust the properties so that as many particles as possible will exceed this critical velocity.

This still all leaves the question as to why the particles bond to the substrate and each other. The most generally accepted theory (and the one used throughout this thesis) is related to the formation of adiabatic shear bands (ASB). Those particles that have high enough kinetic energy (velocity is the biggest part) when they collide with the substrate, will undergo severe plastic deformation upon impact. This deformation will create bonds between particles and between substrate. If the deformation is high enough it will cause adiabatic shear bands to be formed. This is a shock compaction type process and impacting particles can further deform those already bonded. The process is a solid-state process and can create these types of bonds because it does not rely on high temperatures and it is a physical deformation that the particles undergo. This means the coating will have the same properties as the powder. Anther important benefit of the GDS technology is that prevents any oxidization of the coating. In fact, it is generally believed that the severe deformation of the particle will “destroy” the thin oxide layer that will surround most metallic particles. This lack of oxidization is another beneficial characteristic of GDS and can be made even more obvious by choosing a carrier gas without oxygen in it.

4 Applications

Cold spray has a wide variety of possible and current applications due to its unique properties. Simply put, it can do things other thermal spray techniques cannot. Due to the low temperature environment, cold spray can incorporate materials with which other thermal spray techniques struggle or fail. These include temperature sensitive (amorphous materials), oxygen sensitive (aluminum, copper, etc), and phase sensitive materials (carbide composites) [2]. This means that the cold spray process can work just as well across a wide spectrum of materials. In addition, since the particles are not

Table 1 — Existing Applications for Cold Spraying

Applications	Examples
Metal restoration and sealing	Engine blocks, castings, molds, dies, weld joints, auto body, HVAC, refrigeration, cryogenic equipment, heat exchangers
Thermal barriers	Aluminum piston heads, manifolds, disc brakes, aircraft engine components
Heat dissipation	Cu or Al coatings on heat sinks for microelectronics
Soldering priming	Microelectronics components and printed circuit boards
Electrically conductive coatings	Cu or Al patches on metal, ceramic, or polymeric components
Dielectric coatings	Ceramic coatings for aerospace, automotive, and electronic packaging
Antistick properties	Deposits impregnated with release agents such as PTFE or silicone
Friction coatings	Rolls for papermaking
Localized corrosion protection	Zn or Al deposits on affected helms, weldments, or other joints in which the original protective layer has been affected by the manufacturing process
Rapid prototyping and near-net manufacturing	Well-defined footprints. Fabrication of parts with custom composite or gradient structures
Biomedical	Biocompatible/bioactive materials on orthopedic implants, protheses, dental implants. Porous coatings of these materials on load-bearing implant devices facilitate implant fixation and bone in-growth, replacing cements and screws
Wear-resistant and decorative coatings	Numerous applications

Table 2.1 Applications and example for GDS technology [1].

superheated they retain their original properties and therefore it is possible to choose powders with the properties that are wanted in the coating. These features and more have led to GDS being studied for and already used in many applications. In fact if you look back to a 2005 paper published by Julio Villafuerte [1] he stated the possible industrial applications ranged everywhere from electronics to automotive to medical and even aerospace. Table 2.1 from his paper lists many good applications and examples of how GDS may be used.

5 Important properties

Some properties of GDS that were either not mentioned or should be highly emphasized are:

- Solid-state process.
- Stress on the substrate is more compressive rather than tensile [2, 4].
- No oxidization.
- Forms adiabatic shear bands.
- High density of coatings possible.
- Generally low deposition efficiency.
- Property of coatings same as powder mixture.
- Can apply wide variety of materials to variety of substrates.
- Can apply composite materials.
- May generate variety of thicknesses.
- Does not require surface preparation of substrate.

References

1. Julio Villafuerte, *Cold Spray: A New Technology*, Welding Journal 5 (2005) Vol. 84 issue 5 pp. 24-29
2. Jeganathan Karthikeyan, *Cold Spray, Advanced Materials and Processes* 3 (2005) p33-35
3. S. Klinkov, V. Kosarev, M Rein*, Cold spray deposition: Significance of particle impact phenomena*, Aerospace Science and Technology 9 (2005) p582–591
4. Anatolii Papyrin*, Cold Spray Technology*, Advanced Materials & Processes, 9 (2001) v159 i9 p49
5. J. Karthikeyan, International Status of Cold Spray Technology, Spraytime Vol. 12 Number 1 (2005) p1-4
6. Centerline limited, http://www.supersonicspray.com/, as of Thursday December 18 2008.
7. Roman Gr. Maev, Volf Leshchynsky, Introduction to Low Pressure Gas Dynamic Spray, WILEY-VCH 2008.

Chapter 3

Introduction to Ultrasonic Testing

1 Importance

Ultrasound is simply defined as the region of the acoustic spectrum above human hearing (~ 20 KHz) to approximately a few GHz. Ultrasonics is than simply using this bandwidth to test. Obviously though that does not really mean or explain anything. Ultrasonics has vast potential in almost any industry in the world and already has a wide array of applications. It is one of the simplest methods of non-destructive testing. This non-destructive aspect is arguably the most important since it can save companies time and money. Before most products can be put on the market it must be shown to meet whatever durability requirements it needs to fulfill in everyday use. The most common way to test this is to simply take several samples and physically test them to see how they maintain under normal and overloaded conditions. However, these physical tests have the disadvantage of destroying the samples that are being studied. Not only that, but just because several of the samples are good, it does not guarantee all of the produced product will match. However, through non-destructive testing it is possible to relate the properties of your signal (in this case ultrasonic) to the physical properties of the material. Once a basic standard for what physical properties are required and what ultrasonic data are related to these physical properties, it is a simple method of testing the samples. This allows for complete confidence in the product put forth and saves the expense of destroying some potential products.

Now that the benefits of non-destructive testing have been established, what is so special about ultrasonics? While it is true that there are many types of non-destructive

testing methods (X ray, laser etc) ultrasonics is one of the simplest, safest and least expensive methods available. In addition, most materials allow for the propagation of ultrasound through them thus enabling this method to be used for multiple materials. This is especially important for this thesis as mentioned in the previous chapter cold spray allows for the deposition of multiple types of materials on a variety of substrates.

2 Waves

As with anything, it is good to establish the basics first. Ultrasonic waves are not a physical object that travels through a material, more they are a disturbance that is propagated through instead. This is because it is actually the atoms of the material that propagate the wave. This ultrasonic wave or disturbance causes the atoms to vibrate within the material leading other atoms to vibrate and thus propagate the wave through the material. Before expanding on this, it is important to mention that ultrasonic waves can be generalized into two main types: transverse and longitudinal [1]. A transverse wave is shown in figure 3.1. The main requirement for this type of wave is that the vibration of the atoms is perpendicular to the direction the wave is propagating. Similarly in figure 3.2 it can be seen that the main characteristic of a longitudinal wave is that the vibrations and propagation are parallel (it is important to note that it can be molecules of a material not just air). This work almost exclusively focuses on longitudinal waves though things do get a bit more complicated with the focused transducer (more later).

It has been noted that the wave propagates through a material as a disturbance; however, what controls this disturbance? The simplest answer to that is a

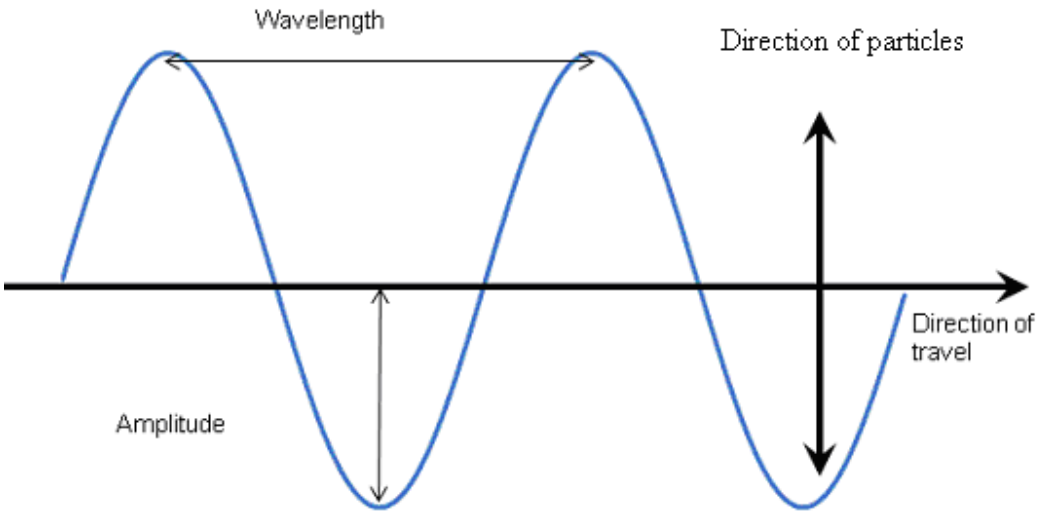

Figure 3.1 Transverse wave.

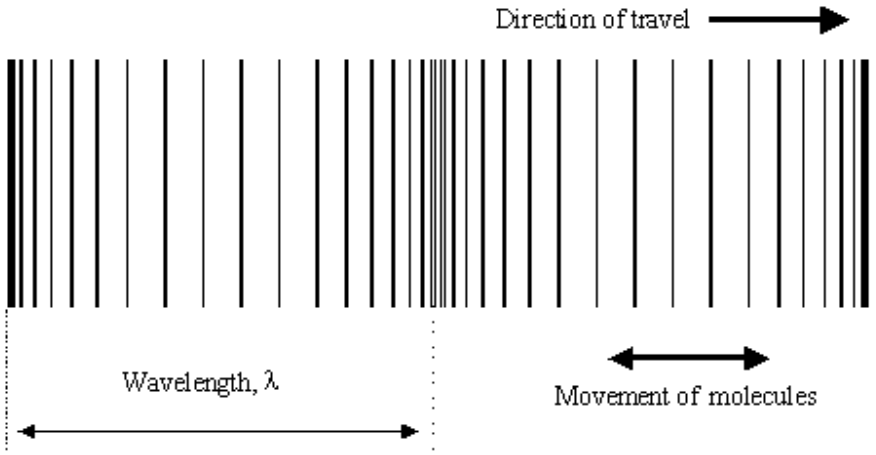

Figure 3.2 Longitudinal waves.

combination of the properties of the material and the wave itself. The physical/geometric aspects of the material that can affect the propagation of the wave will be addressed at the end of this chapter. However, there is one basic property inherent to all materials that is extremely important to ultrasonics and that is the acoustic impedance (Z):

$$Z = V\rho \qquad (3.1)$$

where V is the velocity of the ultrasonic wave in the material, and ρ is the density of the material. This property can be defined as how resistant a material is to the passage of an ultrasonic wave. Materials with high acoustic impedance may not allow for propagation or the propagation might diminish and fade within a short distance. Table 3.1 lists some impedance values for selected materials.

As stated above it is also important to consider the effect the wave itself has. The main parameter of the wave is the frequency (f) or wavelength (λ) which are related by:

$$f = \frac{c}{\lambda} \qquad (3.2)$$

where c is the speed of sound in the material (for air 343 m/s). Thus it is clear that the smaller the frequency the larger the wavelength and visa versa. So than what is the "right" wavelength to use? Obviously, that will depend on the experiment but there are a few key ideas to keep in mind. A smaller wavelength will allow smaller details to be

Material Name	**Acoustic Impedance** (×10^5 gm/cm2 sec)
Air	~ 400
Aluminum	8.17
Aluminum Oxide	26.28
Copper	20.21
Glycerine	2.34
Iron	25.3
Lead	7.81
Nickel	26.68
Sodium	1.84
Tin	12.2
Titanium	14.06
Water (20 C)	1.483
Zinc	17.18

Table 3.1 Impedance values for various materials[2, 3].

recorded (the wave will reflect of features/flaws only when they are near the same size). This also means unfortunately that the wave may not propagate as far in the material since it may encounter obstacles that impede it. A larger wavelength will be more likely to propagate; however, it is possible to miss some of the finer details or flaws within the material. Therefore, it is very important to balance the wavelength such that it will propagate successfully within the material while still being able to detect all features desired.

3 Couplant

When the transducer generates the ultrasonic wave it will not immediately propagate into the sample. It is necessary to have some coupling fluid between the transducer and the material. A simple explanation for this is to consider the impedance values in table 3.1. It was said that these values could be considered as a materials resistance to the propagation of an ultrasonic wave. The value of air is approximately 400 (dependant on temperature), thus if there was air between the transducer and material no wave would be likely to propagate through. However, a common coupling material is water and it can be seen immediately the much smaller value of approximately 1.483 (dependant on temperature) will be much more likely to allow propagation. Anther more proper explanation comes from equation 3.2. For higher frequencies, the wavelength will get very small. It will eventually be smaller than the distance between two air molecules and thus will not be able to propagate in air. In this study, water was used as a coupling fluid for the scanning acoustic microscope and glycerol was used for the flat transducers.

4 Transducers

The transducers used in this thesis may be generalized into two main groups: focused transducers and flat (contact) transducers. While a detailed description of how these transducers work would be well beyond the scope of this chapter there is some main features that should be mentioned. The focused transducer is as its name describes. It focuses the acoustic signal to a single point on the sample. This transducer type was always used as part of a Scanning Acoustic Microscope (SAM). Again, an in-depth study would be to long; however, it is suffice to say the SAM is robotized to scan the transducer in the x and y planes over the sample. For all SAM (focused transducer) measurements, samples were placed in a water bath to use as a coupling fluid. The flat or contact transducer works quite differently. As the name implies, it is flat and is usually kept in contact with the sample. The transducer will generate an ultrasonic signal across its entire face (channel surface) and the obtained results will be an average of this. Saying the transducer is in contact with the sample was actually an oversimplification. As figure 3.3 shows it is necessary to have a delay line between the transducer and sample. This delay line is commonly made out of some simple polystyrene material with low acoustic impedance. Lastly, it should be noted it is still required to have a coupling fluid between

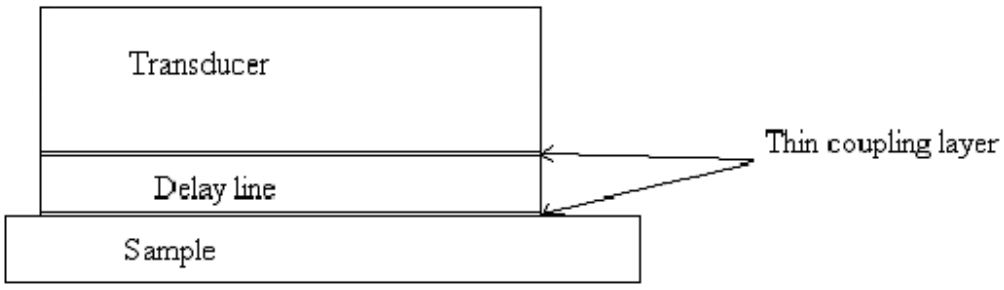

Figure 3.3 Setup for flat transducer measurements.

the transducer-delay line interface and delay line sample interface. For all flat transducer studies, glycerol was used.

One last important detail to consider with the transducer type is that each transducer will have a set value or range of frequencies for which it works. Thus, it becomes crucial to define a frequency range within which the work will be conducted. This requires consideration of the properties of our coatings. The coatings are often multi component materials with pores that can range in size. In addition, the sprayed particles themselves are on average 50 μm but could range up to approximately 100 μm. Finally, the coatings are usually several mms; however, they can sometimes be as small as a few hundred μms. The wavelength will need to be larger than the particle/pore size so that it can propagate through the material without being deflected/lost and similar order of magnitude as our thicknesses in order to guarantee a good reflection/detection of the signal. Thus, by these considerations the wavelength should be on the order of hundreds of micrometres. From equation 3.2, it is clear the sound velocity must also be considered. The most commonly used materials are copper and aluminum composites and they normally have sound velocities approximately 4500 m/s and 6000-7000 m/s respectively. Using equation 3.2 and solving for the frequency based on these velocities and a wavelength of .3 mm than gives values of 15 MHz (copper) and 20-23 MHz (aluminum). Thus, using a frequency range of 15 – 25 MHz would be ideal. However, a wider range (i.e. 3.5-50 MHz) could be used to test different resolutions and to check that the ideal range is indeed being used.

5 Modes

One aspect that has not been discussed yet is how the data is obtained. It was said the transducer generates an acoustic signal that propagates through the coupling fluid into the sample, but how does the data get acquired? Once again, this can be split into two main ways or modes of study. There is the transmission method as well as the pulse echo method. The transmission method is arguably the simplest but least useful. It uses two transducers, one on either side of the sample. The one transducer will generate the signal that propagates through the material and the other transducer will record this signal. Pulse echo however is shown in figure 3.3. It uses a single transducer to create and receive the signal when it is reflected back. This leads to some obvious advantages for the pulse echo method. While the design is obviously more complex, it also requires less hardware (1 transducer only). The value of this technique becomes even more obvious when considered from an applications aspect. The transmission method requires access to both sides of the material being studied. In many non-destructive business applications, this may be difficult if not impossible. Thus, the pulse echo method is a lot more practical from an applications viewpoint. These types of considerations led to the choice to use only pulse echo method for all trials.

There is still the question as to what type of data is obtained and how is it made useful. First, note that the signal that is obtained after propagation will be changed from its original state through its interactions with the material. Thus, the properties of the material are contained within this new signal. The key point to consider though is the type of data that is obtained. The data obtained will be in the frequency domain. However, this is not especially relevant for most academic or business settings.

Therefore, it is necessary to perform a fast Fourier transformation to transform this data into the time domain [4]. The types of data that can thus be obtained will be discussed in the next section.

6 Scans

Once the data is obtained, there is a wide variety of ways it can be utilized. Different types of scans or images can be composed to show the same data in different ways. To help describe the many types of data that can be obtained it will be useful to treat a virtual sample as in figure 3.4. This is a basic example of a coated sample with some uncoated regions and some regions of different thickness. For all cases, the transducer will be placed as shown and thus the signal will go through the substrate first and then the coating. The numbered lines will represent the areas at which the specific

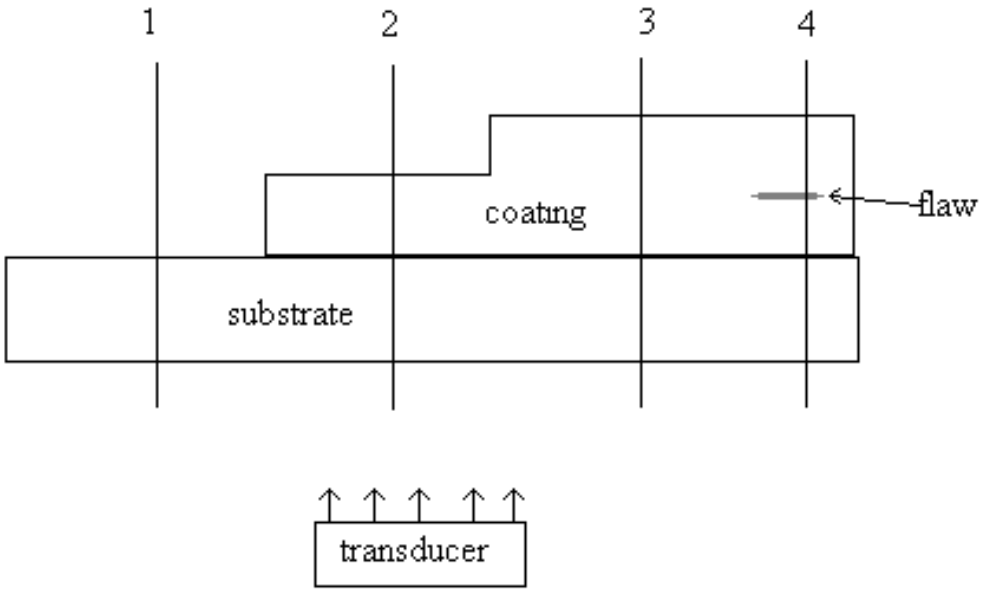

Figure 3.4 Example of coated sample (wavelength of signal much smaller than thickness of substrate and coating).

scan is being done. Finally, we also assume that the frequency used is such that the wavelength is much smaller than the thickness of the substrate and coating otherwise no relevant data will be obtained. The most common way for the data to be first displayed is referred to as an A scan. It shows the amplitude of the reflected signal while the x-axis is the time of flight (time for signal to travel). Examples of A scans that would be obtained for all 4 regions are shown in figure 3.5. The first region will be the same for all 4 since they all have the initial reflection from the bottom of the substrate and than the top. It is clear that region 3 will have its final reflection later since it is a thicker coating than region 2. Finally region 4 shows what can happen if a flaw is there. If it is thick, enough it will block the signal completely (assumed here) otherwise it would just lead to a scan similar to region 3 with an additional reflection at the flaw. One last thing to notice is the difference in amplitude for the second reflection in region 1 as compared to all other regions. The other 3 regions have some of the signal propagate into the coating and thus the amplitude will be smaller.

The next type of scan to consider is referred to as a B scan. This type of scan shows a vertical cross section of the sample at a specific point. Thus if considering the sample in figure 3.4 it would show what the sample looks like if it was cut along one of those lines. Region 4 will make the most promising example. This time however the flaw will be considered not large enough for the signal to be completely reflected. The resultant B scan as well as the new A scan is shown in figure 3.6. The top and bottom of the substrate is clearly shown as well as the coating with the flaw. Again note that the reflection from the flaw will be reduced since some propagates through. Also important is the fact that the signal can become distorted when passing through a flaw as shown.

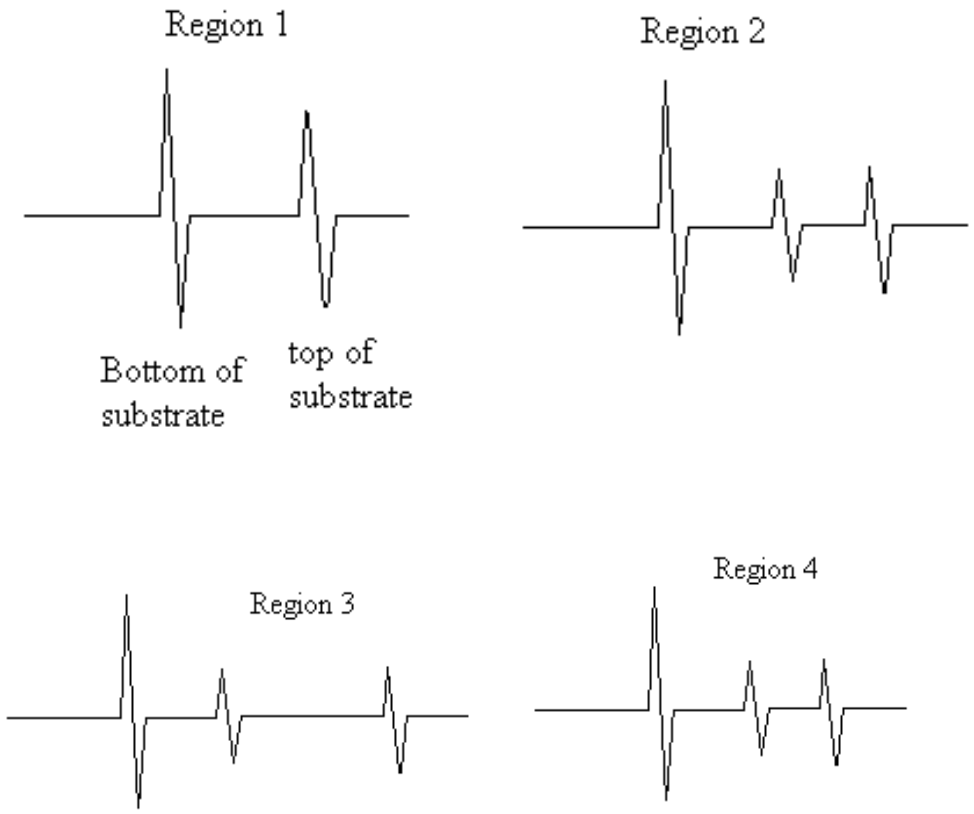

Figure 3.5 Examples of A scans for created sample.

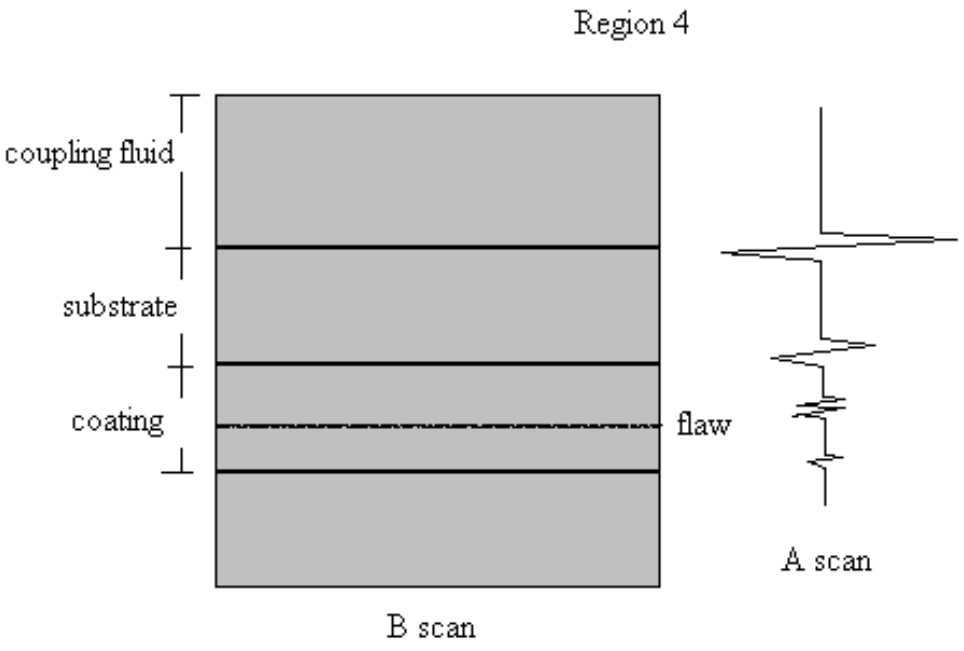

Figure 3.6 Example of B scan.

The third type of scan is referred to as a C scan and it shows a horizontal cross section of the sample at a specific point. This means it would be possible to take a cross section within the coating, substrate or even the interface to study the features. An actual C scan and corresponding B scan (the B scan is taken along the blue line) for a sample is shown in figure 3.7. This was a coated sample and after coating, the bottom of the substrate had 4 holes drilled in it. The left two were conical shaped (as can be clearly seen in the B scan) while the right two were flat drills. These features can be clearly seen. Not only that but it was also easily distinguishable that the second hole from the right actually pierced up and through the coating. This image was created with the transducer on the coated side, thus the signal passes through the coating to the bottom of

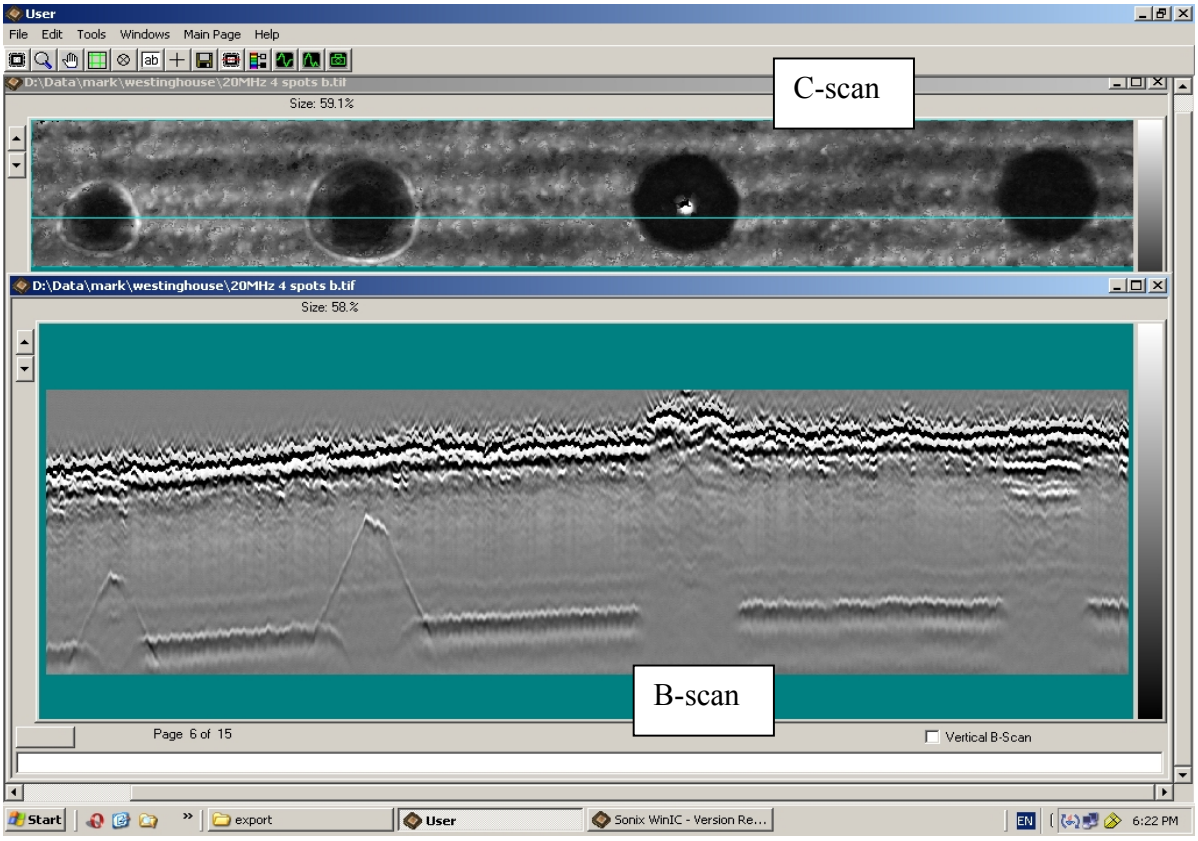

Figure 3.7 Real C and B scans of sample.

the substrate (or top of drilled holes) and reflects back. The C scan is a cross section near the bottom of the substrate. The lines on the C scan are from the peaks and valleys of the coated surface. Finally, it is clear from the B scan that the signal becomes distorted as it passes through the coating.

The final type of scan to discuss is referred to as a D scan an example of which is shown in Figure 3.8. The exact details of this plot is unimportant for now and will be specified later however it still can be valuable to explain a general D scan. Simply, a D scan is multiple B scans over a period of time (time is along the x-axis). Obviously, this type of measurement is only useful during online (during the process) measurement since otherwise the features will not change. However, during online studies it allows for a cross section at a specific point to be monitored and to see how it changes. Again the exact details of the plot is not needed right now but suffice to say it is clear that it changes over time.

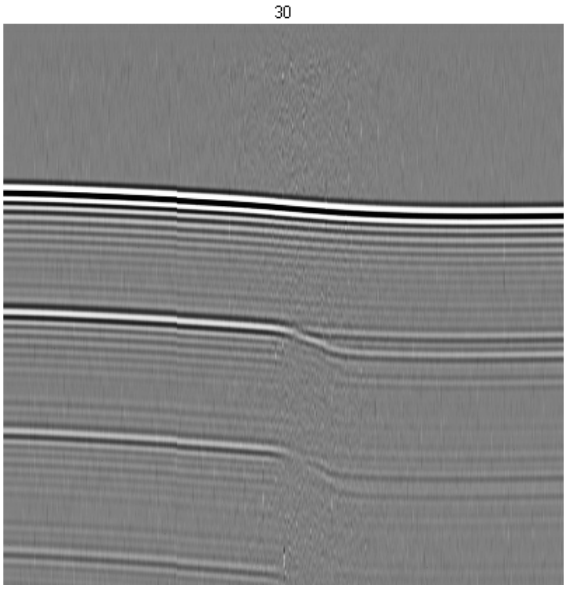

Figure 3.8 D scan.

7 Factors That Can Diminish Performance

The final point that needs to be addressed is which factors can diminish the performance of the ultrasonic signal. The four simplest and most relevant to this type of experiment are expanded upon below [1].

One of the most obvious concerns when using ultrasonic means to study a sample is how rough the surface of the coating is. The ideal case is to have two completely smooth and parallel surfaces but of course, this is not always the case. One important thing to note is that roughness can effect the measurements whether it is on the side where the transducer is coupled or if it is from the reflecting surface. Roughness at the coupling surface would obviously pose some major problems. It prevents perfect coupling at that surface and some regions may have pockets of coupling fluid. These pockets could distort the results or even reflect part of the signal away. In addition, if the opposite surface is rough it can cause the signal to be distorted. With an uneven surface, it is more difficult to determine exactly when or where the signal reflected from and some of the signal may be reflected at odd angles and lost (figure 3.9).

Also important is the way the transducer is coupled to the sample. This is especially important when considering the contact transducer that was most commonly

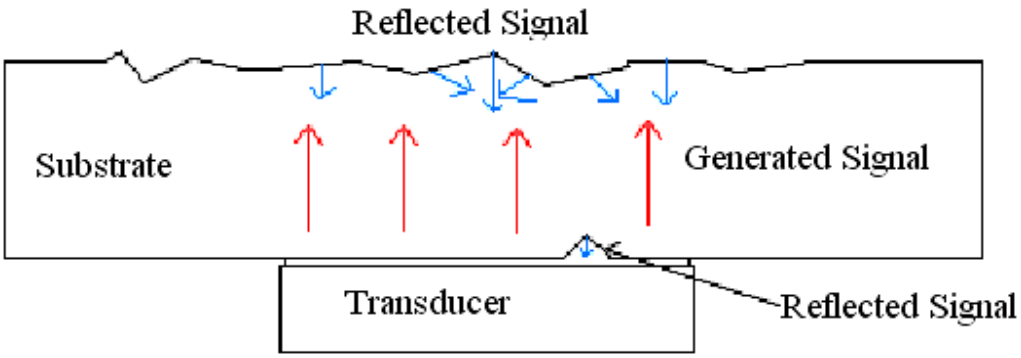

Figure 3.9 Signal lose due to rough surfaces.

used throughout this work. If there is to much couplant or is built up in one region more than another it could cause a misread in the delay time at that point or even cause the transducer to be on angle. This would cause a loss of some of the signal and improper readings. Finally it is important for a contact transducer to use the same pressure (when pressing the transducer against the sample) otherwise the amount of coupling fluid will be uneven between trials. For these reasons, it is very important to guarantee there is good contact and full coverage of the entire ultrasonic surface.

Another important point to consider is whether the sample is curved at all. This curvature could cause some incoming signals to be deflected at odd angles and lost (figure 3.10). This is important to consider since the edges of the samples tend to curve towards the substrate and in this region some of the signal may be lost thus it is important to attempt readings at regions that are more "flat".

The last point to consider is the acoustic properties of the coating itself. A porous coating can cause significant scattering and loss of the signal (figure 3.11). To overcome this sometimes it is necessary to increase the wavelength to minimize the effects these flaws have on the signal. Finally, it is also important to note possible velocity variations

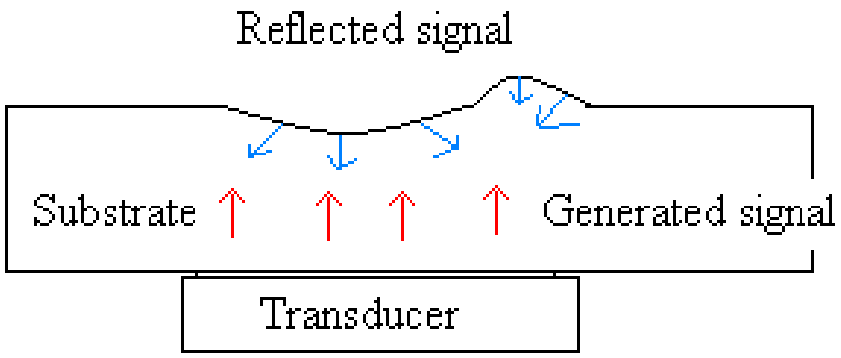

Figure 3.10 Signal lose due to curved surfaces.

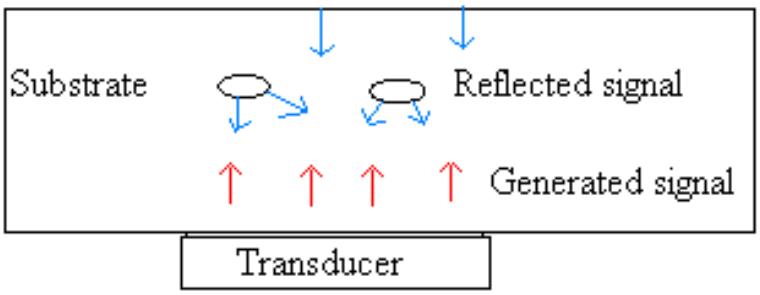

Figure 3.11 Signal lose due to porosity.

within a coating. This is simply describing that within a sample it is possible to have regions with slightly different velocities. This becomes a much more significant issue when dealing with composites as in this case. The different materials will have different velocities and some regions will have different materials. For this, it is necessary to chose materials that will hopefully spray near homogenous coatings and furthermore it is necessary to study some pure materials as a check.

References

1 http://www-group.slac.stanford.edu/tf/NLCTA/notes%20Fritz%20Caspers/Ultrasound.pdf as of March 25, 2009

2 http://www.signal-processing.com/tech/us_data_liquid.htm, as of Friday December 19, 2008.

3 http://www.inficonthinfilmdeposition.com/en/densityandacousticvalues.html, as of Friday December 19, 2008.

4 Albert S. Birks, Robert E. Green, *Nondestructive Testing handbook,* American society for nondestructive testing 1991.

Chapter 4

Young's Modulus of Cold Sprayed Composites: An Analysis Based on a Minimum Contact Area Model

1 Introduction

The cold or Gas Dynamic Spray (GDS) process is a type of thermal spray technique that relies on the high velocity of particles rather than on high heat. The severe plastic deformation of particles during GDS processes results in both the consolidation and strengthening of the resultant coating. This suggests that the extensive plastic flow of a particulate material is the main process that governs the structural formation of the coating. The metals are well known materials, which in many cases exhibit excellent ductility and low flow stress. Metal particles with high kinetic energy build up a dense coating due to deformation upon impact [1]. Thus, the macroscopic mechanical properties of composites are strongly conditioned by the bulk properties of the constituents; they are also influenced by the mechanical behaviour of the matrix/reinforcement interfaces.

A detailed analysis of the bonding process has been undertaken by Borchers et al. [2, 3]. As shown in this study of the interfaces in High Pressure GDS process, inter-particle bonding areas do not form a complete bonding network. In fact, some of the bonding areas exhibit microstructural features such as jets.

Using Transmission Electron Microscopy (TEM), several remarkable features are noted at the interface [2, 3]. In some locations within Al, there appears a tangled structure, where the interface has bifurcations; here, a thin stripe of material with a thickness of some nanometres seems to be interlaced. The Al particles interface is, in

fact, somewhat wavy on the order of some 100 nm, with the grains having low dislocation density. The grain size near the interface is about 500 nm. Copper coating GDS also exhibits a non-equilibrium grain boundary, which is characterized by ultrahigh dislocation densities adjacent to the grain boundaries. The microstructural features of Ni GDS coatings are similar to those of Cu. The particle-particle interfaces consist of nanosized grains and large grains with coffee-bean-like contrast, which is typical for shock-consolidated structures [4].

The above-described results clearly show that effective inter-particle bonding takes place only in local areas. Moreover, the structure of the bonded areas is not uniform, influencing the interfacial mechanical properties as well. It seems reasonable to classify the inter-particle bonds as those made by i) the melting of adjacent particles, ii) adiabatic shear band formation with a phase transformation at the inter-particle contacts, and iii) adhesion (van- der- Waals) forces.

At present time there are two primary issues of GDS that have not yet been completely defined: i) the type of inter-particle bonds, and ii) the surface area occupied by the definite type of inter-particle bonds that are created by the appropriate powder consolidation technique. The primary bonding structures (described above) may be characterized by definite macroscopic mechanical properties. Thus, based on the analysis of the mechanical properties, the structure of inter-particle bonds and the contact surface area data, it may in fact be possible to estimate the contribution of each bonding mechanism to the mechanical strength of the composite as a whole. Therefore, having characterized the inter-particle bonding mechanism, it seems that it will be possible to

determine the i) macroscopic bonding strength, ii) bonding surface area, and iii) bonding area structure.

An in-depth analysis of the interfacial mechanical properties of GDS sprayed materials has not yet been performed from this perspective. The most detailed information characterizing the bonding of Al, Cu, Ni and Ti may be found in a series of papers by Borchers et al. [2, 3] for HPGDS processes. These authors apply the Prummer [5] classification of bonding mechanisms in samples prepared by explosive compaction. The authors uncover three main bonding types:

(1) Adiabatic welding – the main bonding mechanism in the technique of explosive cladding. This bonding is characterized by adiabatic shear instability and jet formation at the welding interface. Prummer [5] calls this bonding "explosive welding", but since cold gas spraying is not a technique where explosive are used, we use the above expression in this work.

(2) Friction welding – here shear bands form which are not necessarily an adiabatic shear instability.

(3) Liquid phase sintering – the near-surface areas of the powder particles melt during compaction and subsequently weld together during cooling.

To find adiabatic welded interfaces, one has to look for jet formation caused by adiabatic shear instabilities. Although it is not as easy to certify jet formation in Low Pressure GDS (LPGDS) as it is in explosive welding, narrow bands of metallic materials observed between two particles could be evidence of jet occurrence (see Figures 4.1 and 4.2). In addition, the plicate appearance of inter-particle region on the SEM micrograph (Figure 4.3) may further suggest jet formation during LPGDS.

According to some [3], the microstructure of High Pressure GDS (HPGDS) Copper coatings is characterized by a narrow zone of dynamically recrystallized material around the particle-particle interfaces. Further, they find no evidence for microstructural

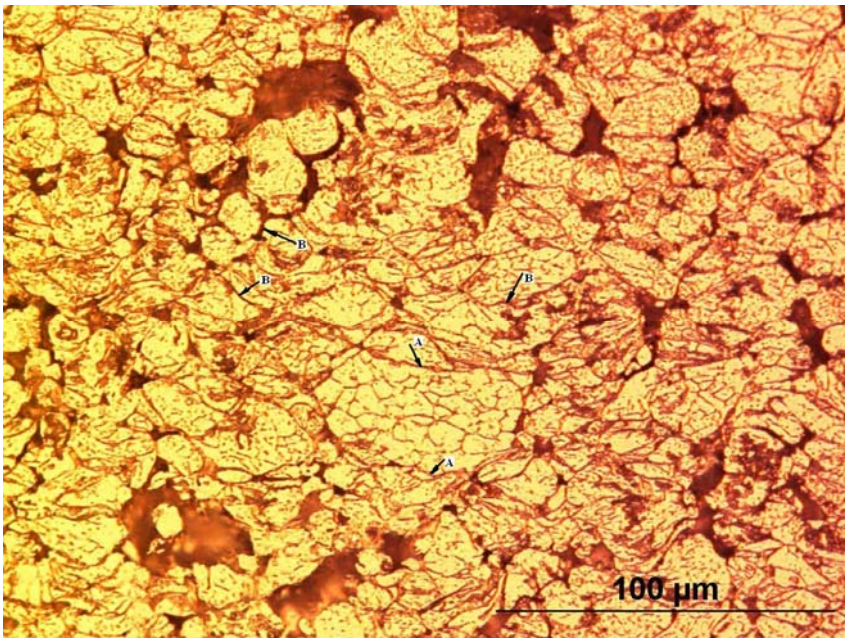

Figure 4.1. Microstructure of aluminum Low Pressure GDS coatings.

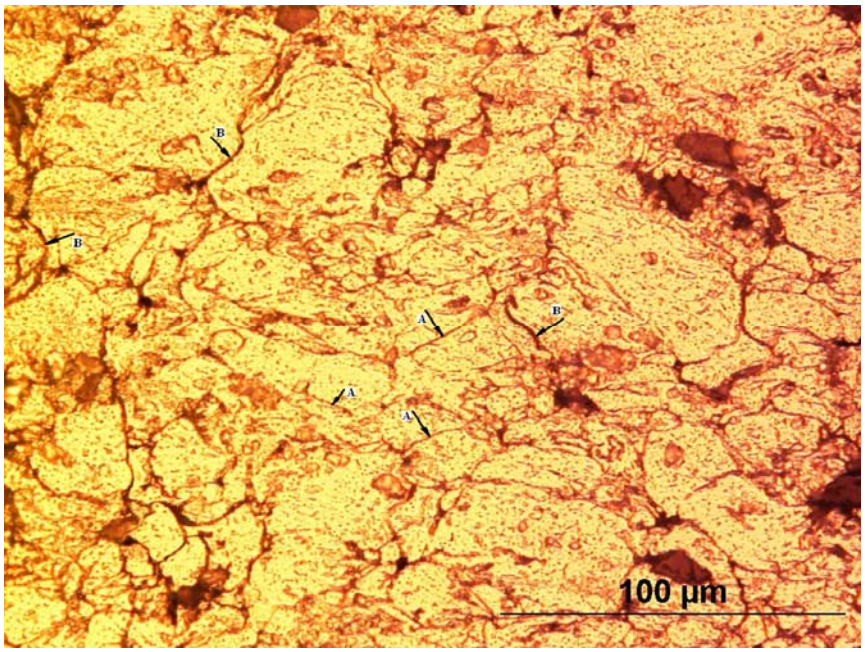

Figure 4.2. Microstructure of aluminum and 10% alumina Low Pressure GDS coatings.

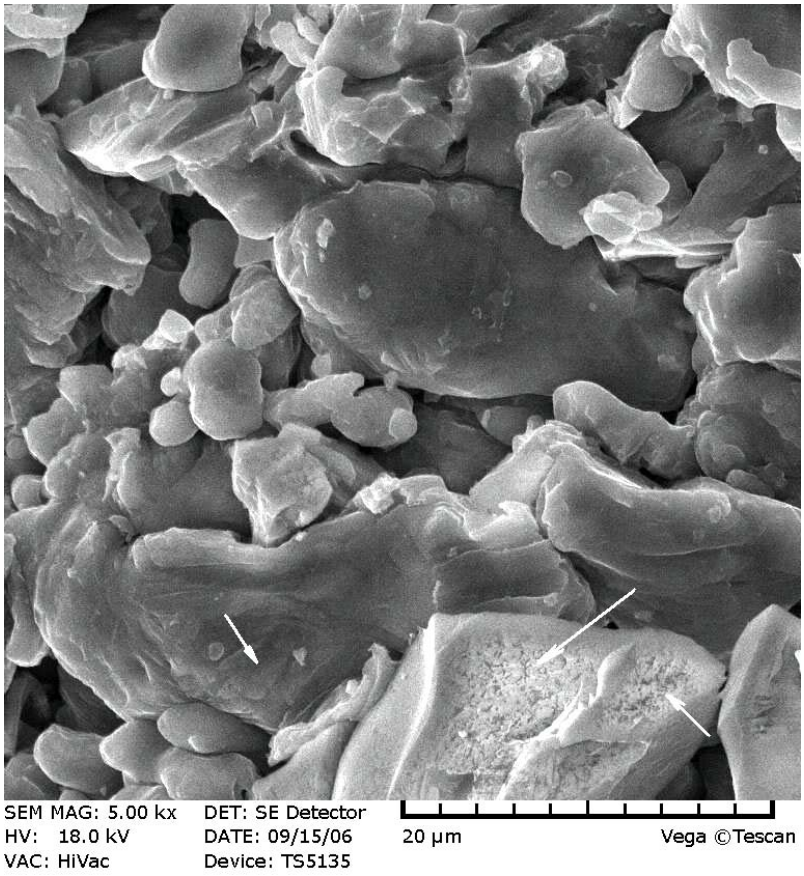

Figure 4.3. SEM of Aluminum and 10% alumina fracture surface.

phenomena related to melting. Despite numerous studies [6], there is a decided lack of data concerning the microstructure characterization of composite coatings made by LPGDS. Of specific interest is the current lack of any studies on the elastic modulus of LPGDS.

2 Experimental procedure

2.1 Materials description

A large variety of Metal Matrix Composites (MMCs) are employed, but by far the most widely studied materials are Al metal matrix composites. MMCs that are reinforced with ceramic particles offer high strength and a high elastic modulus, as well as favourable

high-temperature properties as compared to the corresponding monolithic materials used as the matrix. The exact nature of the GDS technique used in the fabrication of MMCs has a significant effect on the overall properties of the product. Severe deformation of the particle interface due to shear instabilities must be achieved in order to obtain effective bonding between the matrix and the reinforcements.

Composite designation	Particle designation	Average particle size	Porosity	Volume fraction of reinforcement	Interparticle distance
		μm	%	%	μm
Al- Al_2O_3-1	Al_2O_3	10	3.1	10	187.5
Al- Al_2O_3-2	Al_2O_3	10	3.5	15	100.
Al- Al_2O_3-3	Al_2O_3	10	4.3	30	44.6
Al- Al_2O_3-4	Al_2O_3	45	4.9	50	10
Ni-TiC-1	TiC	20	7.5	10	90
Ni-TiC-2	TiC	20	8.1	20	57.1
Ni-TiC-3	TiC	20	9.5	30	33.3

Table 4.1. Composite microstructure characteristics.

Aluminum, Copper and Nickel are the most common matrix elements employed in metal-ceramic composites; on the other hand, the most effective reinforcement particles are Al_2O_3, SiC, TiC and others. For example, it has been reported [7] that the addition of TiC as a reinforcement improves the mechanical properties at both moderate and high temperatures. The composites chosen for this study are shown in Table 4.1.

It is widely recognized that the strength of the particle/matrix interface is of great importance with respect to the toughening of materials. In fact, the stiffness of the metal matrix is greatly increased by the presence of rigid particles. This has numerous additional advantages including an increase in both exploitation temperatures and thermal conductivity, as well as generating a larger coefficient of thermal expansion.

2.2 Preparation of samples

First, commercially available Al and Ni were blended homogeneously with reinforcement powders Al_2O_3 and TiC respectively. By varying the average size and chemistry of the reinforcing ceramic phase (Table 4.1), diverse composite microstructures were obtained. Prior to spraying, the substrate surface was sandblasted using 300 mesh alumina grits. The substrates were then cleaned with acetone and methanol, dried in hot air and weighed before and after GDS. The composites were then sprayed using a portable apparatus equipped with an SST Centerline gun [8] to produce seven composites, which will be referred to hereafter as shown in Table 4.1. This system utilizes the injection of powder into the divergent part of a supersonic nozzle. The powder mixtures were supplied by a powder hopper and were injected into the supersonic portion of the nozzle near the throat area by means of a negative pressure developed by an accelerated stream of compressed air passing through the nozzle. The injected particles are accelerated in the high velocity air stream by the drag effect. To increase the air velocity and, ultimately the particle velocity, the compressed air can be preheated within a range from 100^{o}C to 700^{o}C. The pressure and temperature of the compressed air were monitored by a pressure gauge and a thermocouple positioned inside the gun. The

gun was installed on an X-Y manipulator to scan the air-powder jet over the substrate surface. The compressed air pressure was kept constant at 0.5 MPa. The particle velocities at the exit plane of the supersonic nozzle, as measured by a Laser Doppler Velocimeter, were in the range of 550-650 m/s. The powder-feeding rate was varied in the range of 0.5 to 1.5 g/s, while the standoff distance (measured from the exit of the nozzle to the substrate) was held constant at 10 mm. A rectangular nozzle with an exit aperture of 3.5 x 10 mm was used. Finally, the coatings were removed from the substrate for later analysis.

2.3 Determining the elastic modulus

Determining the value of the elastic modulus required two steps. First, a portion of each sample was used to determine density. Using a YDK01 (Sartorius) density determination kit and the Archimedean principle the density was determined to within an accuracy of 0.1%. The remaining portion of the samples was used to determine the longitudinal velocity of sound. The samples were ground and polished to give two parallel surfaces. The samples were then studied using an AM 1102 acoustical microscope (Tessonics) utilizing a 20 MHz flat transducer with a 3 mm diameter. Due to the porous nature of the material, it was undesirable to immerse the samples, and therefore Imagel R03-GEL1 (Tessonics) was used. The velocities were than determined by multiple trials (to prove accuracy) of the pulse echo overlap method.

Finally, using the experimentally determined values for velocity (v) and density (ρ), it was possible to determine the elastic modulus from:

$$E = \frac{v^2 \rho (1+\nu)(1-2\nu)}{(1-\nu)} \qquad (4.1)$$

where v is Poisson's ratio, which we assumed was approximately .3 for all cases.

3. Effect of porosity on elastic constants – Minimum contact Area model

In order to increase the strength and stiffness of the composite materials, the reinforcement particle loading must be as high as possible. However, previous studies have shown that local reinforcement particle clustering might become a serious problem when the reinforcement loading is very high, e.g., at 30 vol. % [9]. Some ceramic reinforcement particles that may become clustered (e.g., SiC) usually cannot be sintered and bonded together at the consolidation temperature used for Al-based MMCs. Weak bonding between the ceramic particles may play a major role in micro-crack initiation and growth, which can reduce the modulus of elasticity and fracture toughness of the MMCs. Therefore, high-volume fractions of reinforcement particles (> 30 vol. %) are not usually used in current structural composites [9].

The addition of high-modulus particles to a low-modulus metal matrix invariably leads to an increase in the modulus E of the composite over that of the matrix. As shown in Fig. 4, there is a strong dependence of the modulus composites upon ε_j, for Al-based composite reinforced with Al_2O_3 particles. This behaviour has been well documented [10, 11, 12]. Further, a variety of theories have been developed to explain the dependence of E upon ε_j. The one we considered was the Hashin-Shtrikman equation [13]:

$$E_c = \frac{E_m\left[E_m\left(1-\varepsilon_j\right)+E_r\left(\varepsilon_j+1\right)\right]}{E_r\left(1-\varepsilon_j\right)+E_m\left(\varepsilon_j+1\right)} \qquad (4.2),$$

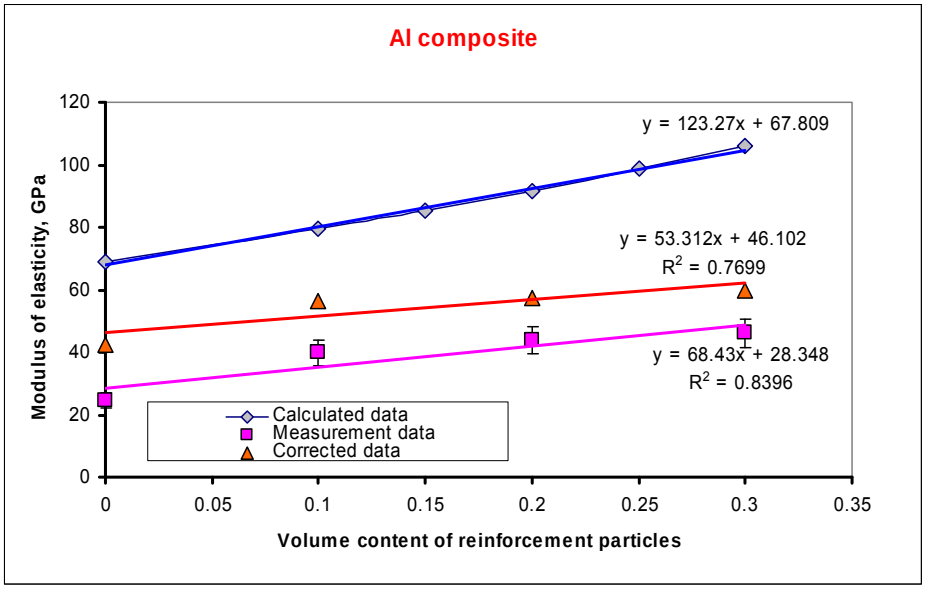

Figure 4.4 Elastic Modulus of Al based composites.

In the case of GDS composite coatings, the porosity has great potential influence on the mechanical properties and, as such, it must be taken into account. Porosity leads to a decrease in the elastic modulus because the load-bearing area of a material is reduced by the pores, with the stress becoming 'concentrated' near the pores [14]. For a body containing a low concentration of spherical pores, the MacKenzie solution [14] for the Young's modulus of the porous body is given by

$$E = E_0\left(1 - Af + Ff^2\right) \qquad (4.3),$$

where E_0 is the Young's modulus of the dense material, f is the porosity fraction and A and B are constants of the order of 1.9 and 0.9, respectively.

The Young's modulus measurement results (Figure 4.4) reveal the dependence $E=f(\varepsilon_j)$, for LPGDS Al based composites is below those calculated with *H-S* model. The corrected data takes into account porosity according to Eq. (4.3) and results in an increase of E. It is important to note that the calculations of E with *H-S* Eq. (4.2) was based on

the assumption that the structure of GDS composites is similar to infiltrated composites described by Kouzeli and Mortensen [10].

In the LPGDS case, the interparticle bonding seems to be characterized by the adiabatic bonding in accordance with Borchers et al. [3]. The adiabatic bonding results in measured sound velocity similar to metallurgical bonding obtained in MMC casting or infiltrated MMC. However, the area of adiabatic bonds at the interparticle contacts constitutes only a fraction of the total area of interparticle contacts. This means that about 35-45% of the contact area does not have real adiabatic bonds, and thus leads to a decrease of Young's modulus. In order to more precisely characterize the formation of the interparticle contacts, it is necessary to analyze, in detail, the actual Young's modulus – bonding area relations.

4 Development of MCA model for GDS process

The central feature of the GDS shock consolidation processes is that energy is dissipated by a shock wave as it traverses a powder medium. Inter-particle adiabatic shear band formation, vortices, voids, and particle fracture may occur due to plastic deformation. Meyers *et al.* [4] describe various energy dissipation processes that take place during shock consolidation: plastic deformation, inter-particle friction, microkinetic energy, and defect generation. If we assume sintering to be an ideal bonding process and characterize bonding by the relation v/ v_o, we may compare our ultrasonic velocity measurement data with theoretical calculations of Mizusaki *et al.* [15] for sintering. In fact, Figures 4.5-4.8 show the sintering process according to a model based on the minimum contact area between particles [15]. In Figure 4.5, the particles are initially

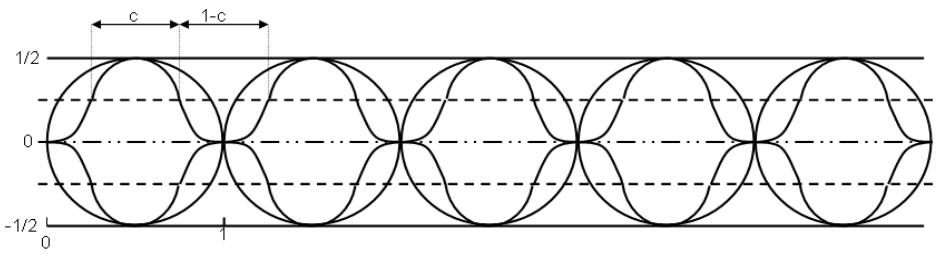

Figure 4.5 Mizusaki model- sine wave approximations [15].

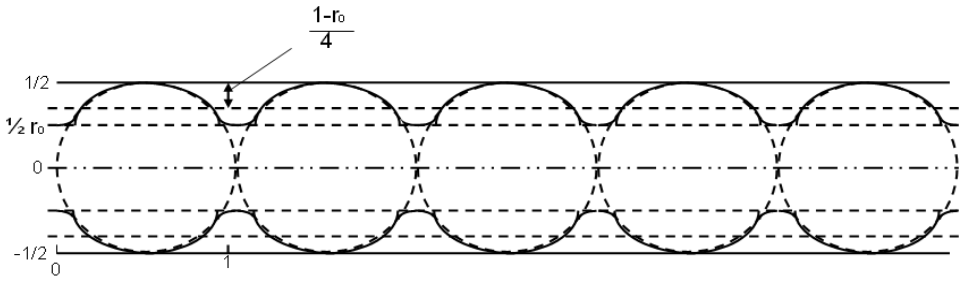

Figure 4.6 Mizusaki model- during sintering [15].

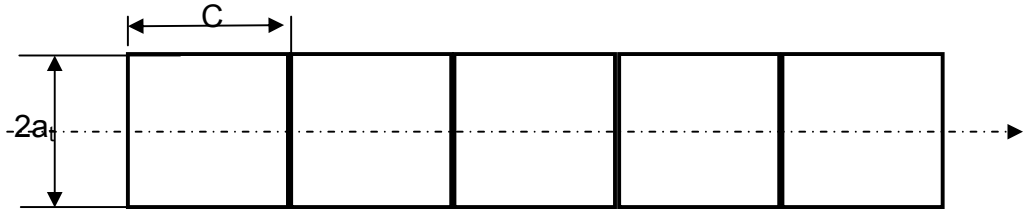

Figure 4.7 Mizusaki model-fully sintered [15].

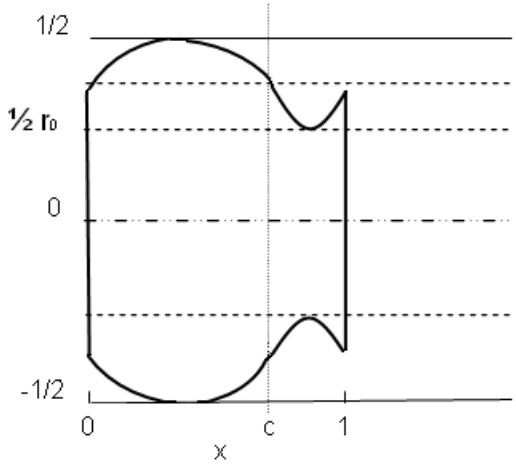

Figure 4.8 Mizusaki model- Relative value interpretation [15].

touching without any deformation. The model uses two *sine* functions to approximate the particle shape at all times. The first sine function represents the inter-particle distance

(given as *c*). The second sine function represents the neck, or area of contact between subsequent particles. The neck is characterized by its diameter r_o and its thickness, 1-c (see Figures 4.5-4.8). Figure 4.6 shows that as sintering takes place, the inter-particle distance will grow, as does the neck. The neck diameter will continue to widen until full density is reached, as in Figure 4.7 where the diameter of the rod is given as $2a_t$. It is unnecessary however, to consider absolute values; in fact, a_t may be taken to equal ½ [15]. Figure 4.7 does show that when full density is achieved, r_o is equal to $2a_t$. Figure 4.8 shows the result of this interpretation using relative distances. The first *sine* function represents the particle from 0-c, while the second function goes from *c-1*.

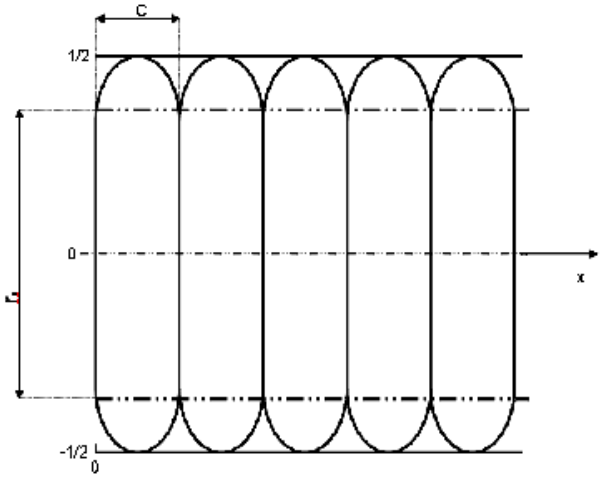

Fig. 4.9. GDS model of densification.

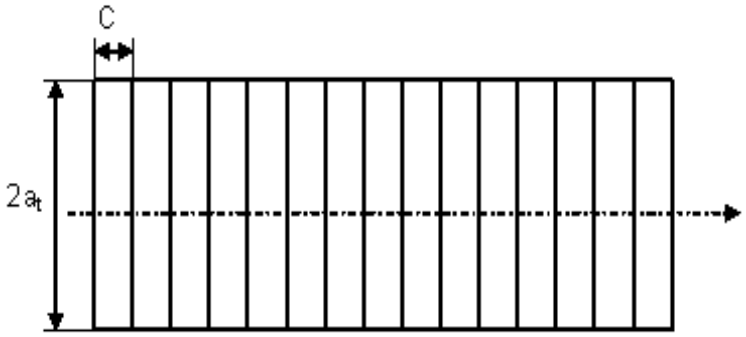

Fig. 4.10. GDS model full density.

A ‘particle column’ model of GDS shock consolidation is shown in Figures 4.9 and 4.10. In this case, only particle deformation is responsible for the increase in neck diameter. The thickness of adiabatic shear bands for the GDS case is considered to be several microns [16]. For this reason, the thickness of the neck is approximated to be zero.

Another notable feature of the GDS shock consolidation model is that the particle deformation process is one in which the volume of the particle is unchanged. Thus, at any moment of deformation the solid material incompressibility equation $V_o = V_i$ is valid. When $a_t = a_o$, the relative density of the particle string (Figure 4.5) is the ratio V_o / V_{io}, where $V_{io} = \pi a_o^2 \cdot 2a_o$.

The pore fraction may be calculated based on a particle string representative element (Figure 4.5):

$$\theta = \frac{V_{pore}}{V_{cyl}} = 1 - \frac{4a_o^3}{3a_t^2 c} \qquad (4.4),$$

where a_t is a radius of circumscribed cylinder. Taking into account $\frac{\rho}{\rho_o} = 1 - \theta$ the relative density is

$$\frac{\rho}{\rho_o} = \frac{(ma_t + nr_o)^2}{16a_t^2} \qquad (4.5),$$

where m and n are the coefficients of approximations that fit the following boundary conditions:

1. if $a_t = a_o$, $r_o = 0$ and $\frac{\rho}{\rho_o} = 0.33 - 0.6$, and

2. if $2a_t = r_o$, $\frac{\rho}{\rho_o} = 1$

A consequence of determining porosity in this manner is that the value obtained will always be a relative value (compared to the full density). This can be seen since we obtain the porosity by subtracting the relative density (density of sample over fully dense case) from 1. Thus, these values will be unit less.

Further adaptations have been made to this theory using results from the works of Mukhopadhyay and Phani [17, 18]. They approximated the normalized minimum contact area to be equal to the relative elastic modulus of the sample. The minimum contact area (*MCA*) is given by the smallest neck diameter. For the case of interest, this occurs when $F(x) = a_t r_0$, giving $MCA = (\pi / 4)\, a_t^2 r_0^2$. The normalized minimum contact area (*NMCA*) is thus r_0^2. For all practical purposes, the *NMCA* is effectively equal to the relative modulus of elasticity E / E_0 *[19]*:

$$NMCA = r_0^{\,2} \equiv \frac{E}{E_0} \qquad (4.6)$$

The GDS process results in real adiabatic bonds that are achieved within smaller contact areas than *NMCA*. Thus, the difference between theoretically and experimentally obtained values for the ratio E/E_0 appears to result from the inter-particle adiabatic bonding of GDS.

5 Results and discussion.

5.1 Structure Parameters

The case of strengthening in particle reinforced metal matrix composites has been extensively studied in the past. Many dislocation models have been designed to account for strengthening in this class of materials. However, most of these models tend to underestimate the strengthening increment in the metallic matrix due to the presence of

reinforcement particles. Some researchers [10] believe that this underestimation is due to the neglect of another, very different contribution to composite strengthening, namely load-sharing. Unlike precipitation or dispersion hardened alloys, the volume fraction of the reinforcing phase in GDS composites is relatively high. In addition, inter-particle bonding areas fail to create a continuous network, as compared with regular MMC produced by infiltrating. In this case, the matrix sheds load to the reinforcement during straining. This concept of "load-sharing" is central to composite continuum mechanics, which predicts strengthening in particle-reinforced composites based on knowledge of the bulk metal matrix properties, the volume fraction, aspect ratio, and spatial arrangement of the particles. Since the MCA model considers the actual geometric distribution of the particles, the concept of load-sharing is inherent within it.

As-deposited composite microstructures feature a near homogeneous distribution of particles in an aluminum matrix with low porosity (Figure 4.11). Ni-based composites have a higher porosity, diminishing the mechanical properties (Figure 4.12). The basic microstructural features of the Al- and Ni-based GDS composites are summarized in

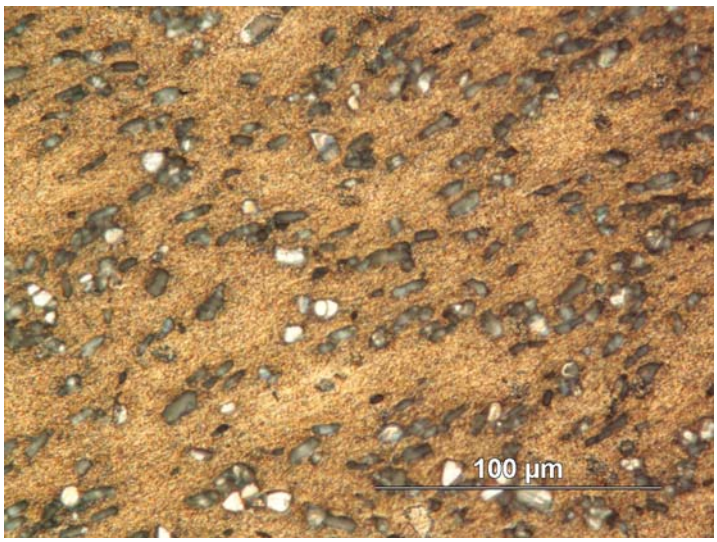

Figure 4.11 Microstructure of as-deposited GDS Al-15%Al_2O_3 composite.

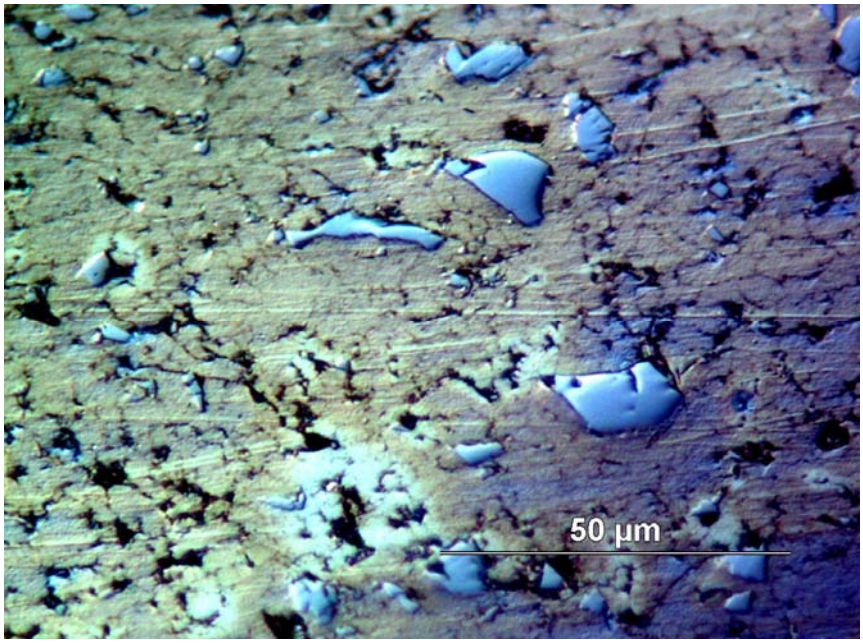

Figure 4.12 Microstructure of as-deposited GDS Ni -30%TiC composite.

Table 4.1. In all these composites, the reinforcement inter-particle distance varies in the range of 10-200 µm, and is comparable with the soft matrix particle size (about 45 µm). Thus, the inter-particle boundaries seem to exert a similar influence on dislocation creation and motion in the matrix, as compared with the reinforcement particles.

5.2 Error determination

One important aspect that has yet to be covered is how precise the measurements are or what is the error (σ). In this type of work, the largest error will actually occur from reading the acoustic data. In chapter 3 the A scan data was shown as perfect peaks (figure 4.13a) that were easily distinguishable; however, this is not always the case. Sometimes the signal that is being read will be less clear and may seem to have multiple peaks spread over a larger time (figure 4.13b). This is especially true when considering coatings with pores or multiple materials that may cause the signal to not propagate

smoothly as in this case. Thus, it is essential to estimate the error that is introduced. To determine the error it is necessary to measure the total time that the pulse takes up (figure 4.13b). If the measurement is taken from the middle of the pulse, the largest error will than be ± half the total time of the pulse. This will account for the peak being anywhere within the pulse. This then gives the error in the time measurement (σ*t). To determine the error in the thickness measurements (σ*d), it is standard to use the reading error. This gives a value of ± .005 mm. Next, to determine the error in the velocity (σ*V) it is possible to use basic error analysis [20]:

$$\sigma * V = V\sqrt{\left(\frac{\sigma * d}{d}\right)^2 + \left(\frac{\sigma * t}{t}\right)^2} \qquad (4.7)$$

where d and t are thickness and time respectively. Due to the high precision of the density measurements, they our considered "perfect" in terms of the error measurements. Thus, the only error dependence that the elastic modulus will have is related to the velocity-squared term. Again, basic error analysis gives:

$$\sigma * E = 2E\frac{\sigma * V}{V} \qquad (4.8)$$

Finally, when considering the relative elastic modulus the only error dependence will be on the experimentally determined elastic modulus. This is because the theoretical value is determined from the Hashin-Shtrikman equation (E_{HS}). Therefore the error in the relative elastic modulus or NMCA (σ*NMCA) is:

$$\sigma * NMCA = \frac{\sigma * E}{E_{HS}} \qquad (4.9)$$

With these equations, it is than possible to calculate the errors for both coating materials. The results are shown in table 4.2. When these values are compared to the

	Aluminum			
Fraction of Reinforcement	0	0.1	0.2	0.3
σE (Gpa)	1.8	2.1	2.2	2.3
σNMCA	0.026	0.026	0.024	0.021
	Nickel			
Fraction of Reinforcement	0	0.1	0.2	0.3
σE (Gpa)	2	2.3	2.4	2.6
σNMCA	0.0095	0.01	0.0099	0.01

Table 4.2 Results of error analysis.

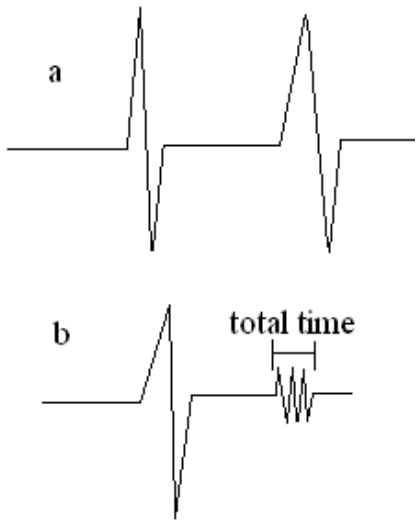

Figure 4.13 a- ideal A scan, b- A scan with non-perfect signal.

experimentally determined results it is clear they should not have a large effect on the results.

5.3 Elastic Modulus and microstructure of LPGDS composites

The microstructures of Al and Al-10%Al_2O_3 GDS coatings (shown in Figures 4.1 and 4.2) reveal that the porosity of the Al coating is significantly larger than that of Al-10%Al_2O_3. In addition, an indication of severe plastic deformation of particles may be clearly seen. It is possible to approximate the degree of inter-particle contact through

their evaluation using an optical microscope. The inter-particle boundaries with adiabatic bonds are believed to be more stable for etching than those with only adhesion (Figures 4.1 and 4.2). The thin grain boundaries within the Al particles may be seen in Figure 4.1. It seems to be reasonable that inter-particle boundaries of the same thickness (for example those shown by arrows A) reveal adiabatic bonding, while thicker ones reveal only adhesion bonding (shown by arrows B). Unfortunately, a quantitative evaluation of the real adiabatic joining area is not possible through metallographic procedures. Neither is the analysis of the fracture topography useful for evaluation bonding, even in spite of the fact that areas of adiabatic bonding are clearly seen on the SEM images (Figure 4.3, shown by arrows).

A quantitative analysis of the adiabatic bonding may be made by comparing the experimental and theoretical data of *NMCA* based on model (4.6). The results of the sound velocity measurement are shown in Figures 4.14 and 4.15. The two main factors that influence sound velocity of the material are density and composition. In addition, the densification process during spraying powder depends on the composition of the powder mixture. An increase in the Al_2O_3 content results in a decrease in the porosity from 0.272 to 0.229; this is due to an intensified plastic deformation of the soft Al particles. This effect is significant only for relatively small contents of Al_2O_3 (up to 10-15%). Further, increases in the content of Al_2O_3 beyond 25-30% result in an increase in porosity due to the considerable change that takes place with respect to inter-particle friction. Al_2O_3 in the shock compaction of a powder layer can significantly affect sound velocity and elasticity modulus parameters (Figure 4.10). This is due to i) a decrease in porosity, and

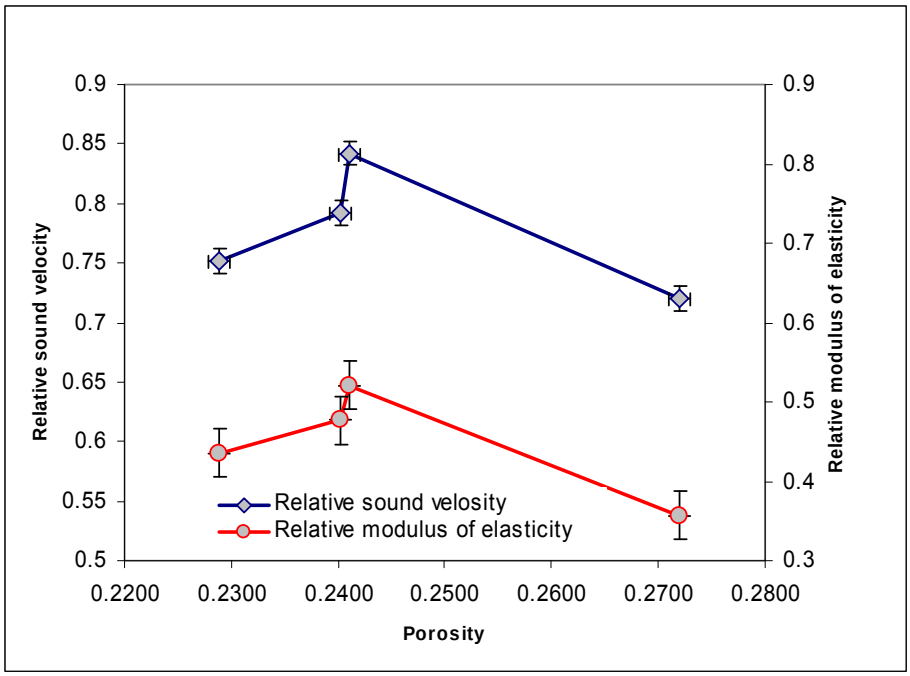

Figure 4.14 Sound velocity of LPGDS sprayed Al composites.

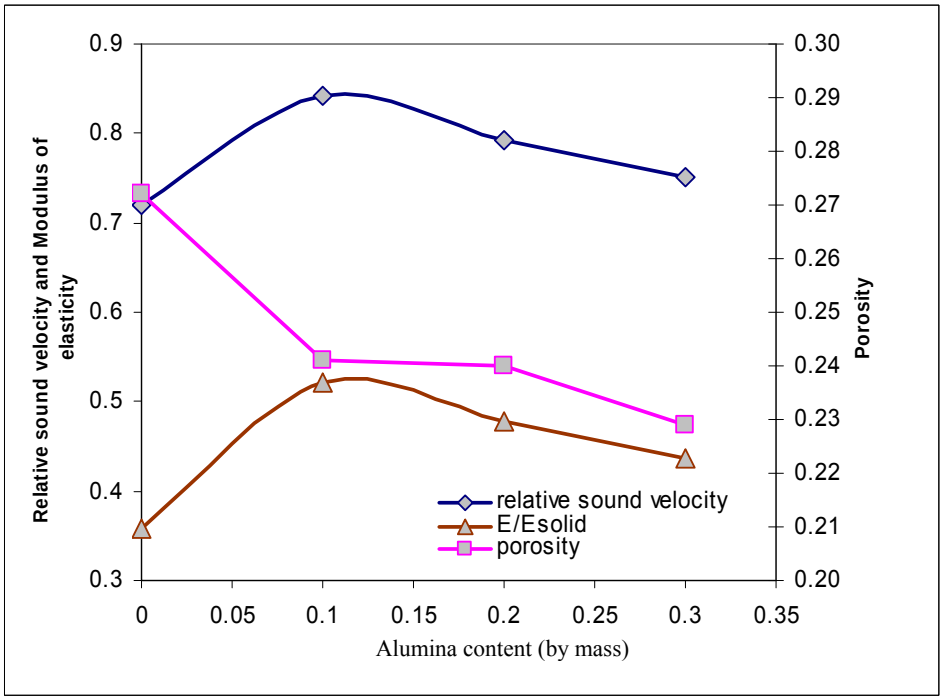

Figure 4.15 Relative sound velocity, Modulus of elasticity and porosity dependences on alumina content in Al/Al_2O_3 coating composites.

ii) severe local deformation of the soft Al particles in the vicinity of inter-particle contact (Figure 4.3, shown by arrows).

The obtained data reveal a change in the mechanism of bond formation at porosities of about 0.2-0.25 (Figure 4.16). The values of real *NMCA* are quite near to those obtained by sintering at high porosities. This means that severe deformation at inter-particle contact results in real adiabatic bonding of particles along the entire contact surface. It is for this reason that the *NMCA* parameter (Eq. 4.6) is measured to be quite near theoretical values calculated in accordance with the Mizusaki model (Figure 4.16). The GDS shock consolidation of the powder layer up to higher density results in an increase in the contact area. However, adiabatic bonding is not achieved at all points. For this reason, the values of *NMCA* do not vary considerably (Figure 4.14, approximation of experimental data).

A simple explanation of this effect is based on the adiabatic shear band (ASB) formation process during GDS shock wave consolidation. In the case of porous powder layer formation, the inter-particle contact area is much smaller than for one of high density. The contact stresses, strains and strain rates are known to be much higher in this case and as such, ASB formation seems to be a highly probable event. When the contact area increases the stresses and strains should decrease. For smaller values of stress and strain, ASB formation is not enough, and the formation of the adiabatic bonds is not achieved. In fact, for porosities in the range of 0.03-0.23, the *NMCA* is about 0.4-0.42 for Al-Al_2O_3 coatings (Figure 4.16). The main characteristic of GDS shock consolidation for small densities (θ = 0.25-0.5) is the localization of deformation, resulting in high values of *NMCA*.

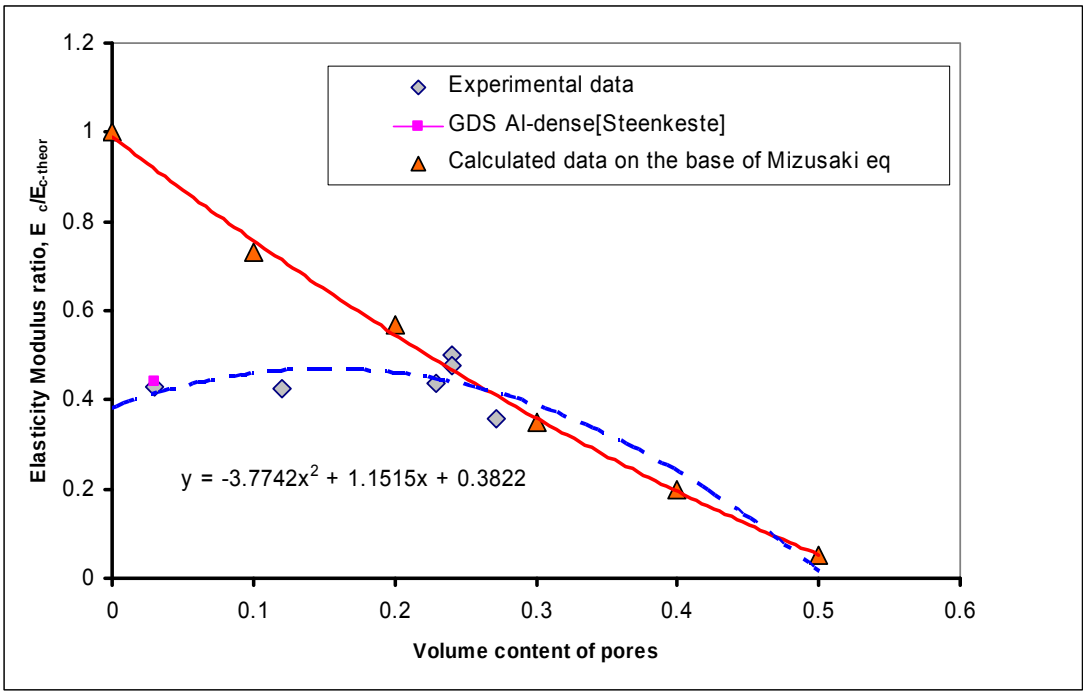

Figure 4.16 Comparison of theoretical and experimental results for relative elastic modulus.

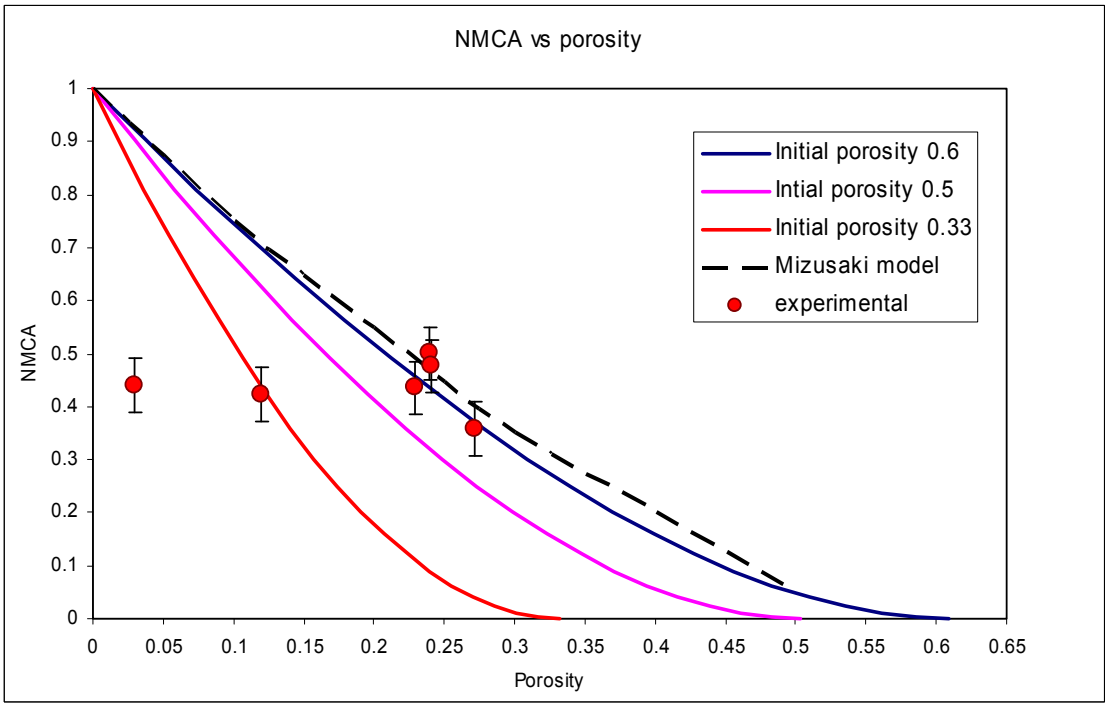

Figure 4.17 Normalized Minimum Contact Area (NMCA) model with various initial porosities as a function of porosity.

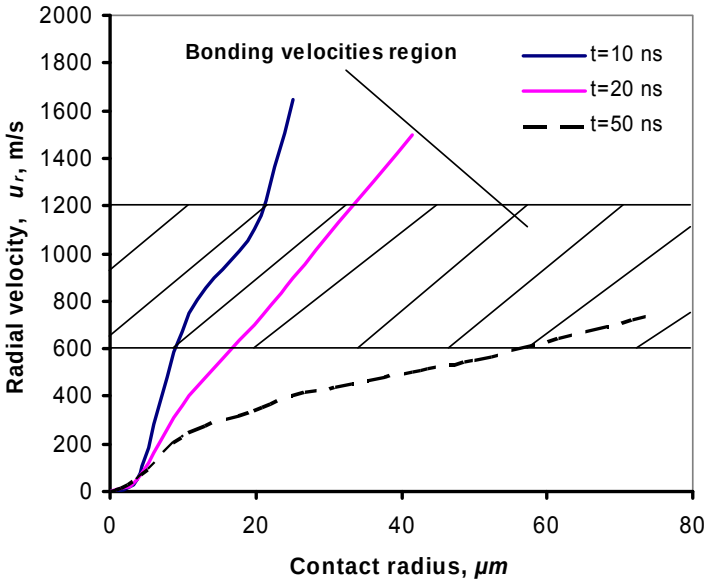

Figure 4.18 Numerical modeling results of impact of Al particle after Papyrin et al. (2002): radial velocity at the interface.

A validation of this model is shown in Figure 4.17. One can see that the suggested shock consolidation model corresponds to experimental data in the range of θ = 0.25-0.5 when the coefficients *m* and *n* of approximation (Eq. 4.5) fit initial porosity θ_o = 0.6. A calculation of *NMCA* has been made using both the shock consolidation model described above and the Mizusaki model. This calculation yields similar results for θ_o = 0.6, however, the curves for θ_o = 0.25-0.5 differ considerably. One can assume that this behaviour is the result of localization effects at higher porosities – indeed, in the last case of higher initial porosity the number of inter-particle contacts is reduced. That leads to an increase in the contact loads and strain rates at the interface between particles.

The numerical modeling results for the impact of Al particles (diameter of particle = 60μm) (Figure 4.18) reveal that the radial velocities are higher than critical velocities only in a small region near the interface. Thus, real adiabatic bonding may only

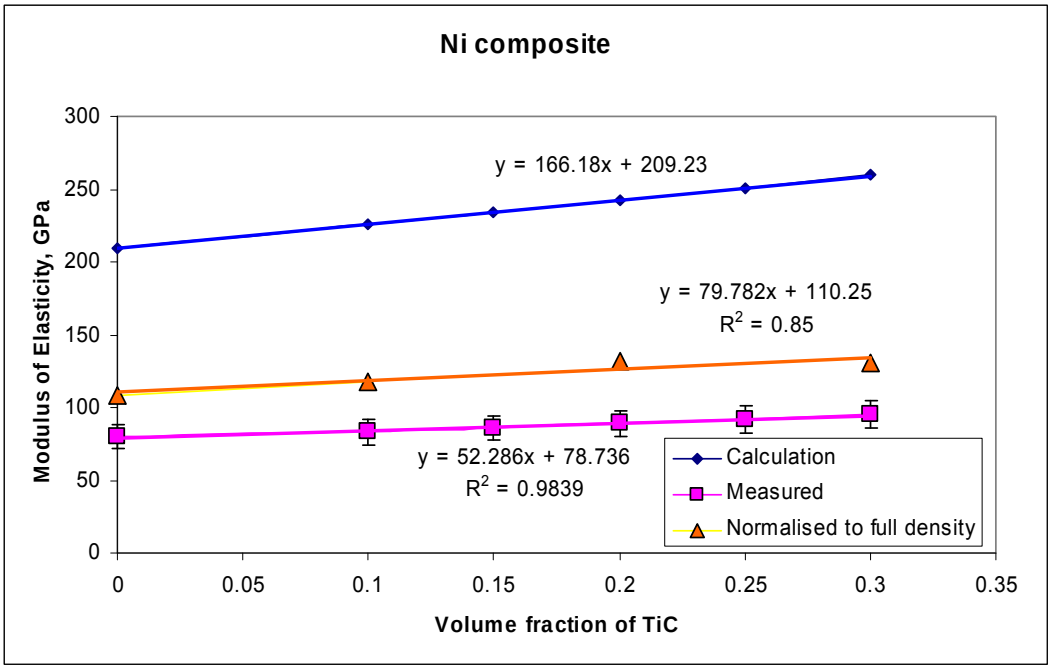

Figure 4.19 Elastic modulus of Ni composite.

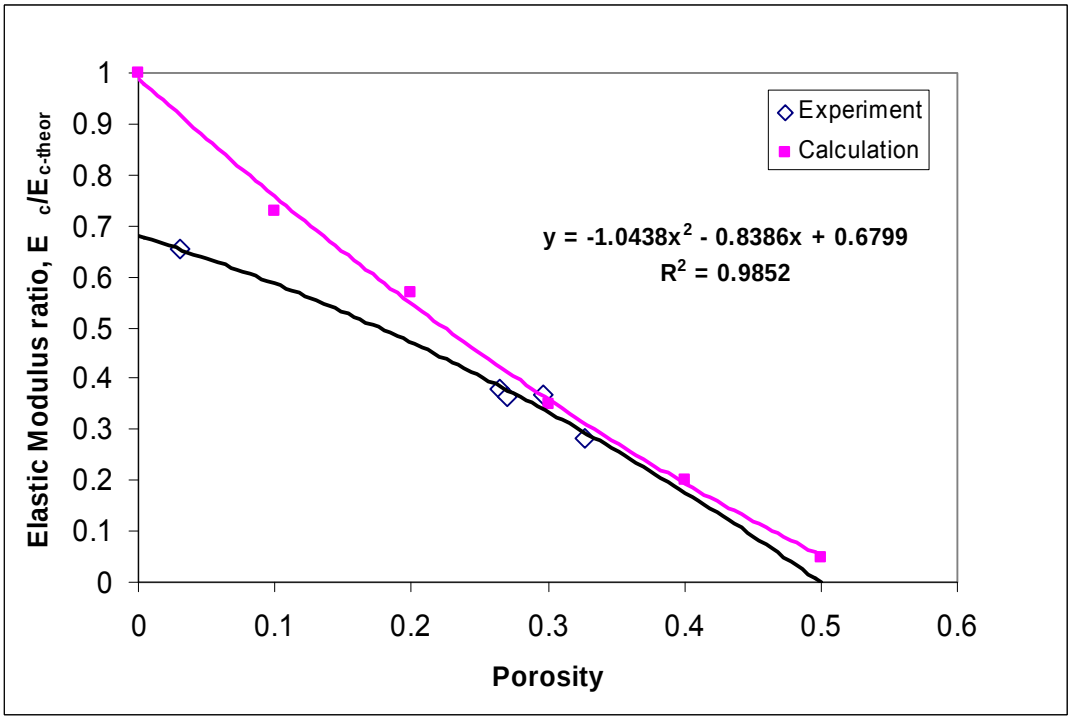

Figure 4.20 Elastic modulus ratio of Ni composite.

be achieved in this area in spite of achieving a tight contact that may be transparent for ultrasound waves. For this reason the *NMCA* value does not completely characterize the area of adiabatic bonding.

A similar behaviour in the *NMCA* function may be observed for Ni-TiC composites (Figures 4.19 and 4.20). Experimental results show that the real modulus of elasticity for LPGDS Al-Al_2O_3 and Ni-TiC composite coatings is only about 40 – 67 % that of the solid material. This suggests that the powder layer shock densification due to LPGDS gives rise to MCAs similar to that of HPGDS [21].

6. Conclusion

The cold spray bonding process was described by a MCA model. By applying this model, a comparison between theoretical and experimental values for the elastic modulus was possible. These values were in good agreement for higher porosity while for lower porosity the lack of full ASB formation reduced the experimental values. This model could prove quite useful for the determination of physical properties such as elasticity for the GDS process, since it relates velocity measurements directly to MCA. This is valuable since the MCA describes the real contact area of the samples. By comparing the theoretical and experimental values of elastic modulus it would than be possible to determine the ratio of bonded area to contact area.

References

1. A. P. Alkimov, V. E. Kosarev, A.N. Papyrin, Dokl. Akad. Nauk SSSR 318 (1990)1062

2. C. Borchers, F. Gartner, Stoltenhoff, H. Kreye, J. of Applied Physics 12 93(2), (2003) 10064.

3. C. Borchers, F. Gartner, T. Stoltenhoff, H. Kreye, Acta Materialia 53, (2005) 2991.

4. M. A. Meyers, D. J. Benson, E. A. Ollevsky, Acta mater. 47, 7, (1999) 2089.

5. R. Prummer, Explosivverdichting Pulvriger Substanzen Grundlagen Verfahrenergebnisse (Springer, Berlin, 1987), in German.

6. R. Gr. Maev, Ev. Leshchinsky, in International Thermal Spray Conference Proceedings, (Seattle, USA, 2006), CD Proceeding**.**

7. A. Contreras, A. Albiter, E. Bedolla, R. Perez, Advanced Engineering Materials 6, 9, (2004) 767.

8. CenterLine (Windsor) Limited**,**http://www.cntrline.com, as on 07 June 2007.

9. F. Tanga, H. Meeks, J. E. Spowart, T. Gnaeupel-Herold, H. Prask, I.E. Anderson, Materials Science and Engineering A 386 (2004) 194.

10. M. Kouzeli, A. Mortensen, Acta Materials 50, (2002) 39.

11. M. Orrhede, R. Tolani, K. Salama, Res Nondestr Eval 8 (1996) 23.

12. H. X. Peng, Z. Fan, J. R. G. Evans, Materials Science and Engineering A303 (2001) 37.

13. D. J. Green, in "An introduction to the mechanical properties of ceramics", (Cambridge University Press, 1998) p. 336.

14. J. K. Mackenzie, Proc. Phys. Soc. London, B63 (1950) 2-11.

15. J. Mizusaki, S. Tsuchiya, K. Waragai, H. Tagawa, Yo. Arai, Y. Kuwayama, J. Am. Ceram. Soc.79, 1, (1996) 109.

16. E. Maeva, A. Aczel, Ev. Leshchinsky, Adiabatic Shear Band Formation in the Gas Dynamic Spray Process*,* Journal for Material Characterization*,* (2006) *(submitted).*

17. A. K. Mukhopadhyay, K. K. Phani, J. Mater. Sci. 33 (1998) 69.

18. A. K. Mukhopadhyay, K. K. Phani, *J. Am. Ceram. Soc.* 20 (2000) 29.

19. L. P. Martin, M. Rosin, *J. Am. Ceram. Soc* 80 (1997) 839.

20. John R. Taylor, An introduction to error analysis: the study of uncertainties in physical measurements, University Science Books; 2nd Revised edition edition.

21. T. H. Van Steenkiste, J. R. Smith, R. E. Teets, Surface and Coatings Technology 154, (2002) 237.

Chapter 5

Preliminary Ultrasonic Study

1 Introduction

The main goal of the thesis is to establish online ultrasonic measurements of the cold spray process. However, first it is necessary to determine which type of transducer to use for the online study. We may generalize them into two types: focused and flat transducers. Focused transducers had the potential benefit of being able to characterize a specific area of the coating (focal point) while the flat transducer averages out the data over the entire channel area. The flat transducers can thus pose a significant problem if the channel area is much larger the features of the coating. Thus, it is necessary to test these transducers and see which gives the most reliable ultrasonic data

An obvious problem arises if we wish to use sound velocity as a main characteristic for relating structural properties. For one thing, it will be necessary to determine a theoretical velocity for these composites to compare against. Of even more importance is determining which properties will affect this sound velocity. Obviously if the velocity relies on to many properties or is just highly variable, it would negate the usefulness of online monitoring. Finally, the velocity must be related to structural properties. It needs to be possible to use the acoustic data obtained to draw qualitative as well as quantitative conclusions about coating structure. From the previous chapter porosity is the logical choice since it is a fundamental property of the coating and can influence the other characteristics of the coating. We know that higher porosity leads to smaller contact points between particles and thus less load sharing [2, 3]. This causes higher strain between particles and can have a detrimental effect on the strength and other

mechanical properties of the coatings such as adhesion and elasticity. In addition, porosity can obviously have extreme effects on properties like corrosion protection since it can allow seepage through the coating. Thus being able to measure porosity is useful both in itself and as a way of qualitatively estimating other properties of the coating.

Cold spray posses some unique problems for porosity testing. The process is extremely variable. While the coatings are normally thin, they can range from 10's of microns to several centimetres. Porosity itself can also have a large range, with values as high as 40% to as low as less than 1%. This means the coating can have both closed and/or open (interconnecting) pours. Finally, cold spray has the ability to spray numerous types of materials onto various substrates. This includes using composites, nonconductive materials, polymers, etc as the powder and/or substrate. These key features make some of the more common porosity testing methods such as vapour, electrochemical, and voltage, difficult if not impossible to use. Thus finding a method to determine porosity within a coating is a valuable goal in upon itself. Ultrasonics has many desirable traits, most importantly the ability to test non-destructively. It also has the benefit of being relatively cheap (main cost is equipment), easy to use, and fast (can scan sample or take individual points). Another significant benefit arises from being able to scan through either the coating or substrate and by changing frequencies and transducer design it should be possible to scan most materials and with various thicknesses. Finally, ultrasonics has the advantage that the sound velocity will depend on the properties of the point being scanned; meaning data is obtained for each exact point. The main disadvantage of the ultrasonic method used in this study is that it is necessary

to know the thickness of the coating at the point of interest limiting its usefulness. However, this problem could possibly be overcome later if the results are good.

The current study is meant to establish the relationship between porosity and sound velocity for various composite coatings applied through the low-pressure gas dynamic spray process. This has a twofold purpose. First if a reliable relation is established it could be used to determine porosity non-destructively. Secondly and most importantly, the hope is this study may be used to help establish real-time monitoring of thickness build-up of cold spray material during spraying. This could lead to a better understanding of the build-up and bonding mechanism associated with cold spray.

2 Theoretical Considerations

This chapter focuses on the ultrasonic determination of velocity within a sample, thus it is wise to have a theoretical value to compare against (also in the next chapter this will be required). For these composite materials, the velocity is unknown and therefore we wish to establish the theoretical value for the case of a fully dense sample. This is accomplished by considering the elastic modulus (E) of each material and the amount or reinforcement material added (ε_j). These are the main components of the Hashin-Shtrikman equation [5]:

$$E = \frac{E_m\left[E_m\left(1-\varepsilon_j\right)+E_r\left(\varepsilon_j+1\right)\right]}{E_r\left(1-\varepsilon_j\right)+E_m\left(\varepsilon_j+1\right)} \qquad (5.1)$$

where the subscripts m and r denote matrix and reinforcement respectively. If one than equates this to the following formula for elastic modulus than it is easy to solve for the

velocity:

$$E = \frac{V_o^{\,2}\rho(1+v)(1-2v)}{(1-v)} \qquad (5.2)$$

where ρ is the density of the solid, v is Poisson's ratio, which we assumed was approximately .3 for all cases. The only problem that arose was when considering the copper or aluminum materials since they are a three component composite and the Hashin-Shtrikman equation is only for two components. However, this can be overcome by first treating two components and solving for there combined elastic modulus than setting this as the new matrix when you consider the second reinforcement material. The velocity values obtained differ slightly depending which reinforcement material you consider first therefore both values were obtained and than averaged for the final value.

3 Experimental Procedure

3.1 Materials/Sample Preparation

First, commercially available Al and Cu were blended homogeneously with reinforcement powders Al_2O_3 and zinc, and TiC and zinc. A thin steel substrate was chosen and grate blasting omitted to ease removal of coating from substrate later.

The composites were then applied using a portable apparatus equipped with an SST Centerline gun [4]. This system utilizes the injection of powder into the divergent part of a supersonic nozzle. The powder mixtures were supplied by a powder hopper and were injected into the supersonic portion of the nozzle near the throat area by means of a negative pressure developed by an accelerated stream of compressed air passing through the nozzle. The injected particles are accelerated in the high velocity air stream by the

drag effect. To increase the air velocity and, ultimately the particle velocity, the compressed air can be preheated within a range from 100^{o}C to 700^{o}C. The pressure and temperature of the compressed air were monitored by a pressure gauge and a thermocouple positioned inside the gun. The gun was installed on an X-Y manipulator to scan the air-powder jet over the substrate surface.

3.2 Property Determination

After spraying both the aluminum and copper samples came naturally off the substrate and therefore the experiment was carried out just on the coatings themselves . The first step involved ultrasonic analysis of the sample. Three types of transducers were used. The first type was a simple focused transducer attached to a Scanning Acoustic Microscope (SAM). The second transducer was the same type of flat transducer as used in the previous chapter (diameter was approximately 6-7mm). The final transducer involved a basic flat transducer but the delay line geometry was much more complex. The delay line converged from where the signal comes in to where it propagates into the sample. This gave a flat transducer with a much smaller area being scanned (approximately 1-2 mm).

Using the SAM B and C scans of the samples were created. Also using the A scans at recorded points along the sample the time for the sound wave to traverse the coating was measured. These recorded points were given x-y coordinates relative to a corner of the sample. Next using a depth gauge and two callipers for coordinating the x and y distances it was possible to determine the thickness of the sample at each point.

These time and distance measurements were than used to determine velocity. Both flat transducers were used at the same identical points as the SAM and A scans attempted.

Next, each sample was split into a number of pieces. Using the same x and y scales it was determined what measurements were on which piece. The goal was to split the measurements between pieces evenly, however the breaking process was not very precise and the determination of what measurements were on each piece was carried out after breaking. The next big step was the determination of the porosity of each sample. This involved obtaining both theoretical and actual density measurements for each piece. Because of the porous nature of the samples it was necessary to coat them in paraffin wax (the volume added by the paraffin was accounted for later in the calculations). Now using an YDK01 (Sartorius) density determination kit and the Archimedean principle the density was determined to within an accuracy of 0.1%. The theoretical density for each material was calculated using the rule of mixtures. Using these two values then led to the porosity of each piece. Finally, it was possible to compare the velocity and porosity measurements of the pieces. Two plots were made for each material, the first comparing all velocity and porosity measurements, while the second compared the porosity to average velocity (obtained by averaging velocity measurements on each piece) of each piece.

4 Precision of Measurements

The next thing to consider is the error in the measurements (σ). As in the previous chapter, the largest error will occur from reading the acoustic data. In chapter 3 the A scan data was shown as perfect peaks (figure 5.1a) that were easily distinguishable;

however, this is not always the case. Sometimes the signal that is being read will be less clear and may seem to have multiple peaks spread over a larger time (figure 5.1b). This is especially true when considering coatings with pores or multiple materials that may cause the signal to not propagate smoothly as in this case. Thus, it is essential to estimate the error that is introduced. To determine the error it is necessary to measure the total time that the pulse takes up (figure 5.1b). If the measurement is taken from the middle of the pulse, the largest error will than be ± half the total time of the pulse. This will account for the peak being anywhere within the pulse. This then gives the error in the time measurement (σ*t). To determine the error in the thickness measurements (σ*d), it is standard to use the reading error. This gives a value of ± .005 mm. Finally to determine the error in the velocity (σ*V) it is possible to use basic error analysis:

$$\sigma * V = V\sqrt{\left(\frac{\sigma * d}{d}\right)^2 + \left(\frac{\sigma * t}{t}\right)^2} \qquad (5.3)$$

where d and t are thickness and time respectively. One last important point to note is that

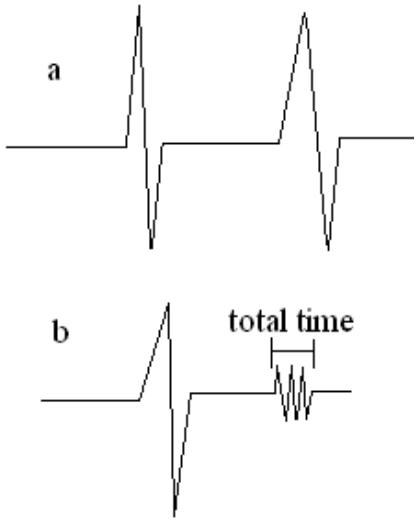

Figure 5.1 a- ideal A scan, b- A scan with non-perfect signal.

due to the high accuracy of the density testing (0.1% accuracy), that error is ignored. As can be seen in the plots this error would not have an effect on the results.

5 Results

The results were not anywhere as promising as hoped; in fact, it was not possible to obtain reliable data for either of the flat transducers. With the basic flat transducer, this was due to the high surface roughness of the coating and the wide diameter of the transducer. The transducer was considering to wide an area and the thickness could differ across that area. The flat transducer with the focusing delay line was simply too complicated. In even ideal circumstances it is difficult to get a strong signal thus with porous structures and a rough surface it proved to be impossible. However, the focused transducer was able to obtain clear enough scans for the work to be continued for this transducer type alone.

Below are the plots comparing theoretical and actual results for the aluminum and copper samples (frequencies were 25 and 15 MHz respectively) with there respective errors. In both cases there does not seem to be any type of clear relationship between porosity and sound velocity. In addition, when studying the plot of all points not just average velocities, one can see (Figures 5.2, 5.3 and 5.5) that the sound velocities can range quite severely even within a piece. Finally, the results (especially for copper) are mostly confined within a small porosity range, yet the velocities vary significantly.

One important point to note is that these values are plotted against relative porosity values and therefore it is possible they do not actually describe the exact geometrical distribution of pores within the sample. While this was at first, a point of

major concern proper considerations may provide a simple explanation. The cold spray process does not necessarily coat all components within a powder equally. In fact, most materials differ in how well they can be applied by cold spray. Zinc is one of those materials that can easily be applied and has a relatively high density. Since both

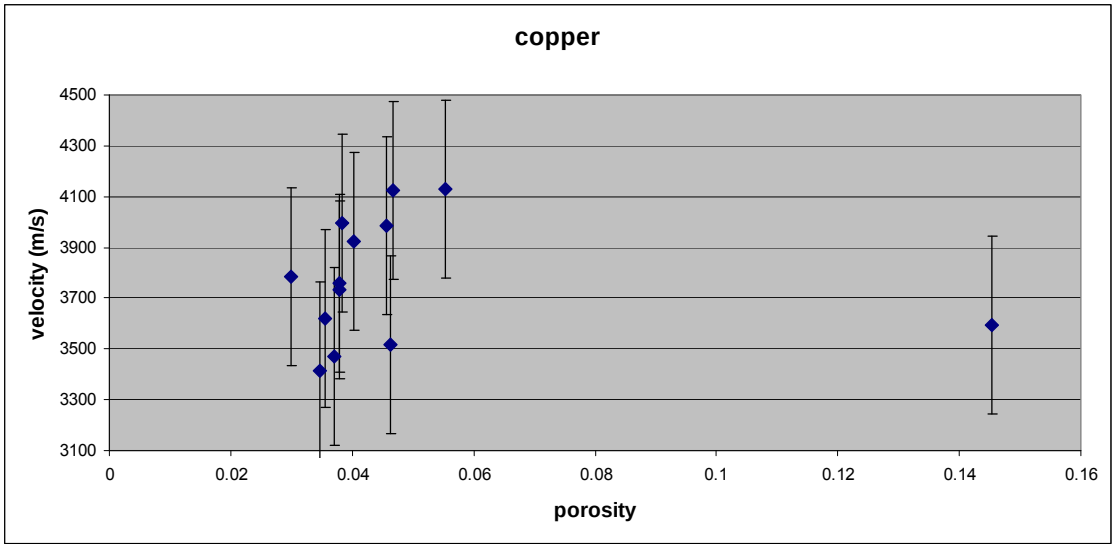

Figure 5.2 Comparison of average velocity and porosity of copper pieces.

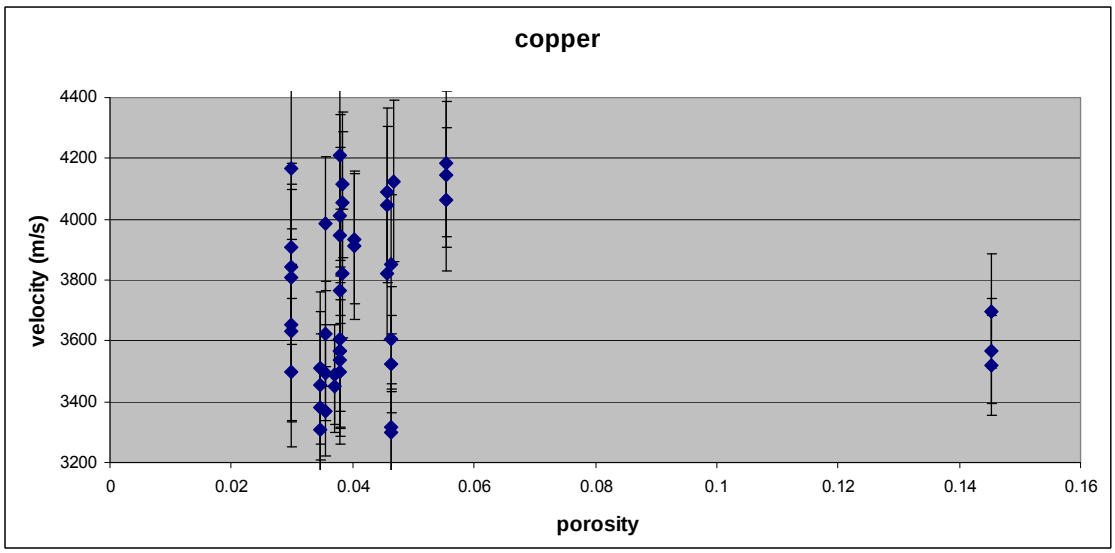

Figure 5.3 Comparison of velocity and porosity for copper.

aluminum and copper powders had a high, content of zinc it seems reasonable to suppose that more zinc bonded and therefore led to a higher density than may be predicted. This is especially important for aluminum as the other two components have much lower density values and thus we may get skewed porosity values compared to the theory.

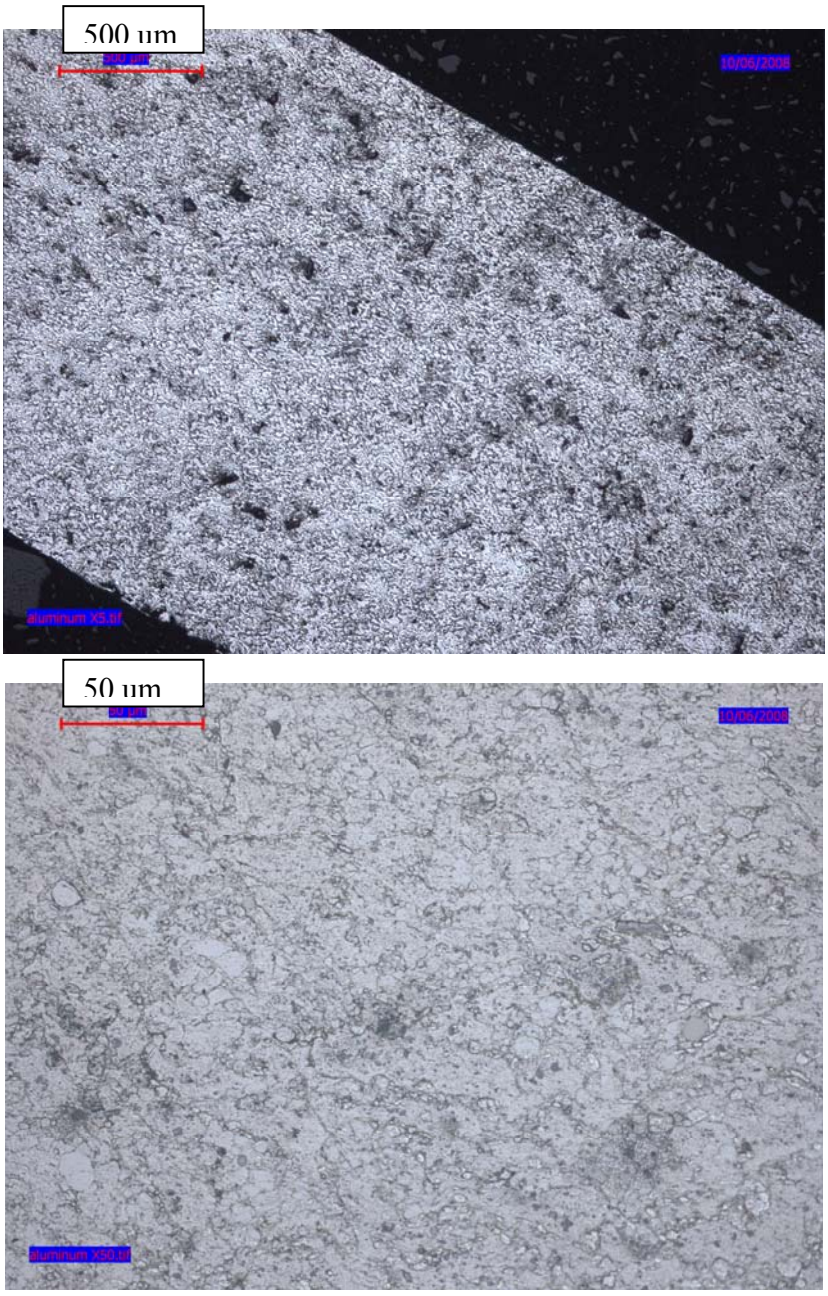

Figure 5.4 Cross section of aluminum showing low porosity (top-50X bottom-500X magnification).

In fact, the original plot for aluminum had much higher porosity values. However, studying the microstructure of Al based coating helps clarify these points (Figure 5.4). The small porosity values of about 6-8% can be seen quite clearly. Fitting our data approximately to these porosity values gives improved experimental results (figure 5.5).

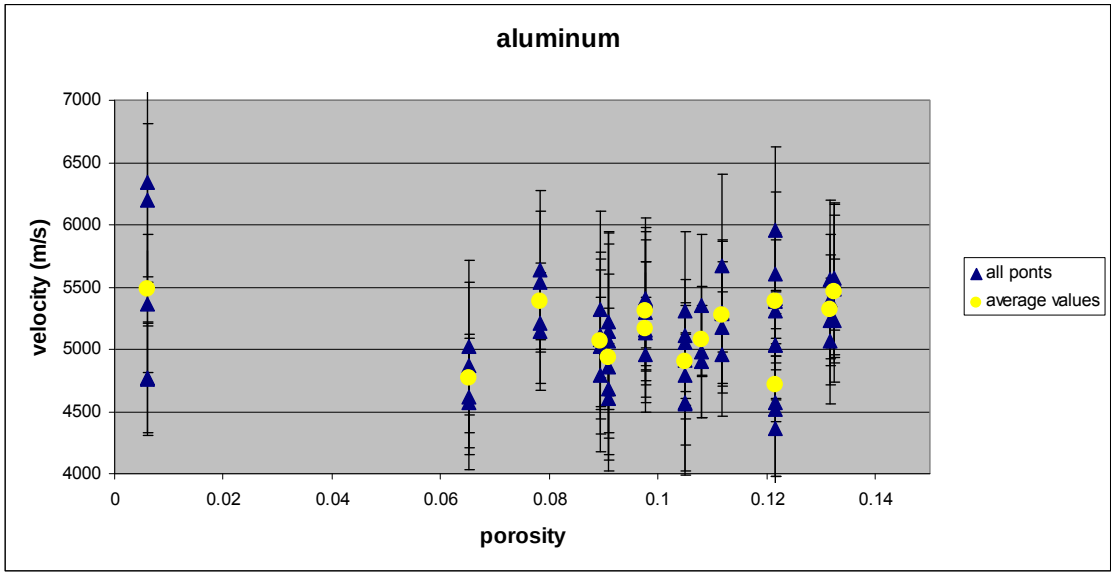

Figure 5.5 Plot of aluminum data points with corrected porosities.

6 Discussion

To be brutally honest, there seems to be no correlation whatsoever between sound velocity and porosity. In fact, for any given porosity there seems to be a range of velocities associated with it depending on point measured. Now the main thing that needs to be determined is whether this is a property of the cold spray coatings themselves or possibly related to the choice of transducer types. The simplest point is again to consider the nonuniformity of the cold spray coating process. It is possible some regions just have more of one type of material bonded than other materials. Since each of these

materials have their own velocity, it is possible to get similar porosity with different velocities. Figure 5.6 shows cross sections of some cold sprayed samples that demonstrates how diverse the structure can be.

To determine whether this is a physical property of the coatings or some other effect it is necessary to get results to compare against. Figure 5.7 shows a plot of sound

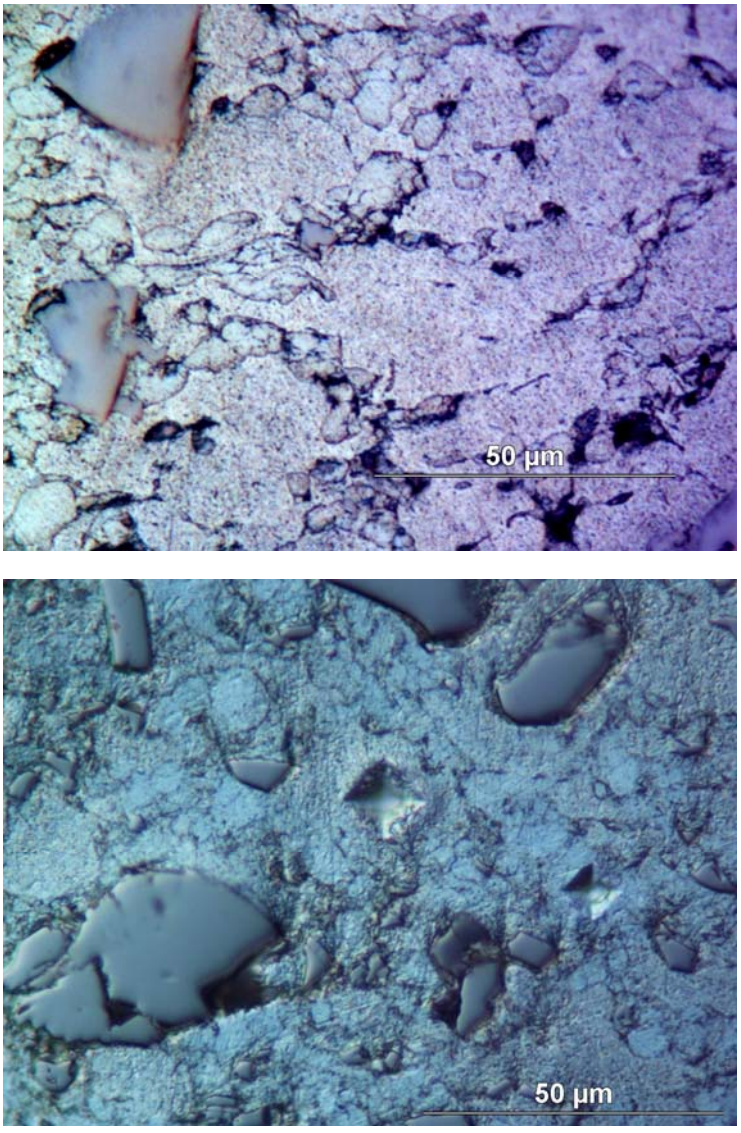

Figure 5.6 Cross sections of cold spray samples showing nonuniformity of coating.

velocity and the respective error for 15 different positions on samples of similar size as above. These samples were aluminum composites (al+25% al_2o_3+10%Zn, and al+30%al_2o_3) sprayed and left on steel substrates. They were than polished to have flat surfaces from which sound velocity measurements using a flat transducer could be obtained. While the porosity values for these samples were not determined, it is immediately clear that the range of velocity values is significantly smaller than those obtained using the focused transducer. It is also clear that the error measurements are smaller as well. Also since the size and compositions of the samples are very similar it is reasonable to expect distribution of porosity values similar to results that have always been obtained. Now before going any further it is important to understand why exactly the focused transducer would lead to vastly different and incorrect results. That answer is actually quite simple if the experiment is closely considered. The goal was to study a coating that is porous, nonhomogeneous, and has high surface roughness. Not only that but the idea was to study this with a transducer that would focus to a point and take all measurements from that point. While hindsight is indeed 20-20 it seems clear now the type of problems that should have been anticipated. Simply put there are too many potential problems for this to work. It has been stated that the transducer will focus to a point but with the extreme properties of the coating, it is much more difficult than usual to guarantee that the focus point is actually where it is wanted. First, consider the porosity. The high porosity throughout the sample could lead to a complete acoustic reflection at a point without it being the top of the coating (a big enough pour near the surface would appear the same and give a much quicker time of travel). Also, consider the high surface roughness, especially for thick or big samples. The thickness of the

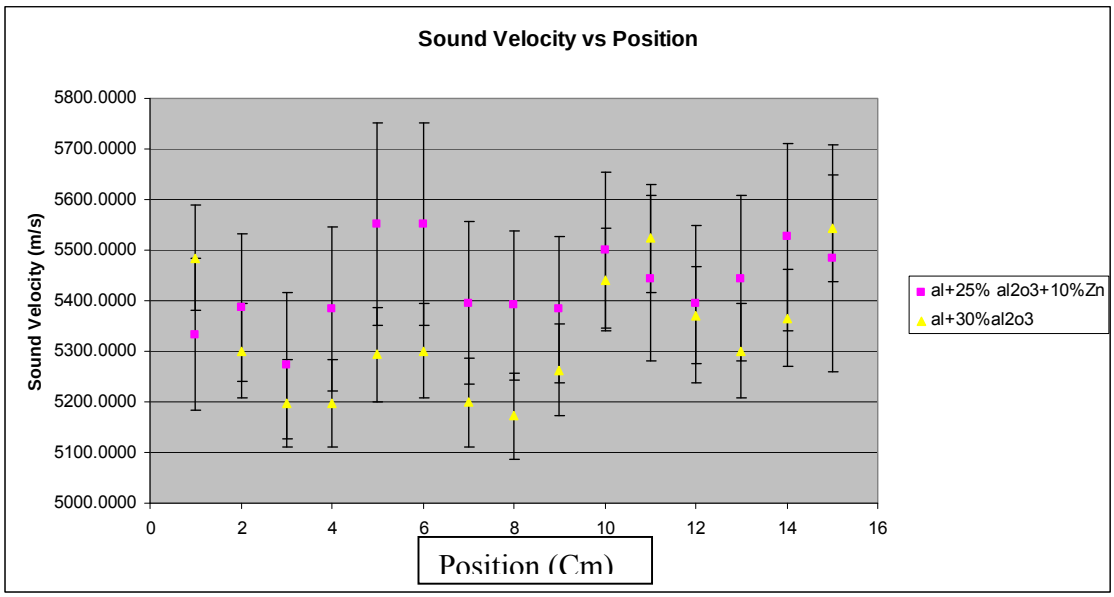

Figure 5.7 Sound velocity readings at different points of samples using flat transducer.

sample can differ vastly even over very small areas. This makes it more difficult to find the exact peak or valley where the transducer focuses on, though hopefully this should not be a big problem if one is

careful. However, this does call to mind a much more severe problem. Since a SAM is used, the focus is set at a certain point within the sample. The problem is that the rest of the sample will not have the exact same thickness and some points may vary by a large margin. This means similar to the high porosity the focus/reflection point may not actually occur at the surface of the coating but somewhere within it (or even an early reflection before it focuses properly). All these factors can contribute to give poor or even incorrect results and would easily explain the wide variety of velocity readings for the focused transducer and not the flat.

7 Conclusion

From the results, it is clear that a focused transducer will not be able to be used for online measurements. However, it remains to be seen the effect surface roughness will have on the results for flat transducers. This will be studied extensively in the next chapter, however to conclude this section it seems imperative to put forth a possible viable method. The most promising technique for online measurement seems to be using a multi channel flat transducer. This is similar to most of the other flat transducers except that it has multiple elements with which to take readings (in essence, many flat transducers in one). This will allow for a much larger amount of data to be recorded as well as allowing dynamic analysis by studying the coating over multiple channels. Finally and perhaps most importantly, this transducer has already been designed and the dimensions for each channel are significantly smaller (diameter of approximately 1 mm) than the other flat transducers that have been used. This will hopefully allow more accuracy since the data recorded per channel will be specific to a small region thus diminishing the effect of surface roughness.

References

1. Mark Lubrick, R.Gr. Maev, F. Severin, V.Leshchynsky, Young's Modulus of low-pressure cold sprayed composites: an analysis based on a minimum contact area model, *J. Mat. Sci. (in press)*

2. M. Kouzeli, A. Mortensen, Acta Materials 50, (2002) 39

3. J. K. Mackenzie, Proc. Phys. Soc. London, B63 (1950) 2-11.

4. CenterLine (Windsor) Limited**,**http://www.cntrline.com, as on 16 June 2008.

5. D. J. Green, in "An introduction to the mechanical properties of ceramics", (Cambridge University Press, 1998) p. 336.

Chapter 6

In Situ Monitoring of Particle Consolidation During Low Pressure Cold Spray by Ultrasonic Techniques

1 Introduction

Cold Spray (CS) is a rapidly developing coating and manufacturing technology in which the spray particles (in the range of 10-150 μm) are fed into a supersonic gas stream accelerated to a high velocity and deposited on a substrate in solid state [1-5]. The severe plastic deformation of the particles on impact produces a deposit that is very dense, with low oxide content and no thermally induced tensile stresses. A typical feature of GDS is the relatively low temperature of driving gas compared with the conventional thermal spray techniques. Accordingly, the temperature of spray particles prior to impact is much lower than their melting point. Other important advantages, especially when compared to thermal spraying techniques are the low oxygen content within the material, the relatively high deposition rates (10–30 kg/h) achievable and the compressive residual stresses after deposition as solidification shrinkage and shrinkage on cooling are avoided. The low temperature characteristic of GDS makes it possible to deposit the coating of the materials without any significant change in the microstructure of feedstock. Most metals, such as Cu, Al, Ti and their alloys, have been deposited by GDS [6-8], and even cermets [9] and ceramic particles [2,10] could be embedded into a metallic substrate to form a thin layer coating.

A glance at the recent literature on different coating processes shows increased interest in depositing composite coatings with precise control of a build-up process. Being relatively new there is not a lot of data describing the build-up process, especially

for the low-pressure case focused on by our group. In fact, other than previous papers by the author *et al*, there seems to be no acoustic measurements of any type. Acoustic studies allow for the non-destructive determination of properties especially if models are developed to relate acoustic and structural properties. Even more important, this paper discusses the development of online monitoring (during spraying) of the process using acoustics methods. The focus is on the thickness build up of the coating and demonstrating the feasibility of monitoring this acoustically.

2 Procedure

Commercially available aluminum (Al), alumina (Al_2O_3), and zinc (Zn) powders were mixed in the amounts shown in table 6.1 (here after referred to by their names in the table). The composites were then applied using a portable apparatus equipped with an SST Centerline gun [11]. This system utilizes the injection of powder into the divergent part of a supersonic nozzle. The powder mixtures were supplied by a powder hopper and were injected into the supersonic portion of the nozzle near the throat area by means of a negative pressure developed by an accelerated stream of compressed air passing through the nozzle. The injected particles are accelerated in the high velocity air stream by the drag effect. To increase the air velocity and, ultimately the particle velocity, the compressed air can be preheated within a range from 100^{o}C to 700^{o}C. The pressure and temperature of the compressed air were monitored by a pressure gauge and a thermocouple positioned inside the gun. The gun was installed on an X-Y manipulator to scan the air-powder jet over the substrate surface.

Name	Composition	Substrate	transducer	Notes
1	Al+10%Al_2O_3	steel	flat contact	1 sample multiple points
2	Al+25% Al_2o_3+10%Zn	steel	flat contact	1 sample multiple points
3	Al+30%Al_2O_3	steel	flat contact	1 sample multiple points
4	Al	steel	flat contact	3 samples off substrate
9 samples	Al+25% Al_2O_3+25%Zn	steel	multi element transducer (1 channel)	9 samples
Online	Al+25% Al_2O_3+25%Zn	aluminum	multi element transducer (1 channel per point)	results obtained during online measurement

Table 6.1 Materials used and particulars of study.

The acoustic studies used two types of transducers but had the same procedure. The ultrasonic probe is attached to the opposite surface of the substrate (except for 4 – pure aluminum the samples broke from substrate). It sends ultrasonic waves through a coupling media and substrate to the area where the spray process takes place (or coating for non-online samples). A hard delay line wetted with ultrasonic gel was used as the coupling media. The wave passes through the substrate, is reflected from the upper surface of the sprayed layer, and travels back to be received by the probe. Measuring the time of flight of the ultrasonic pulse and knowing the sound velocity in the deposited material, it is possible to calculate the thickness of the material at the particular point and time. The main distinction between the two transducers used, was the number of channels/elements (to generate a distinct signal). The flat transducer referred to in Table 6.1 had just a single element generating a 15 MHZ signal and had a diameter of roughly 6.7 mm. The multi element transducer had 52 elements (it is possible to use some and

turn off others) with central frequency and relative bandwidth of the elements 15 MHz and 60 %, respectively. In addition, dimensions are shown in Figure 6.1a. Figure 6.1b shows the dimensions/direction of the applied coating relative to the transducer elements. The grey region is the total coating with lines 1 and 2 showing the middle of the coating and highest point of the coating respectively (more about this later).

As can be seen in the Table 6.1, the samples had a variety of compositions as well as unique ways in which they were studied. For all the sets of samples the time for the signal to propagate within the coating as well as coating thickness were measured (thickness was measured via a depth gauge with accuracy 10μm). The first 3 types of samples were sprayed over large areas, then the top surface was ground and polished to give a smooth surface for sound to reflect back off. They were than studied with the flat transducer in 15 completely separate sections to generate a set of data points. The 4^{th} set of samples had three smaller samples (one data point per) all of which broke from the substrate. Both the top and bottom surfaces were polished and then were studied with the flat transducer. The "9 samples" were a set of three samples that were each cut in thirds leaving 9 pieces. Again, the top surface was ground and polished but this time the studies were conducted using a single channel of the multi element transducer (each piece correlated to one data point). The final "online" samples were the most important. These acoustic measurements were conducted during the actual spraying process. The setup for this online monitoring is shown in figure 6.2. The multi element transducer sits in the middle cavity on a spring with a ball bearing on top and two screws are used to tighten the substrate against the transducer. The spring keeps the transducer in tight contact with the substrate, while the ball bearing sits against the middle of the transducer to guarantee

the transducer is parallel to the substrate. The spray is than simply directed diagonally across the sample and over the transducer while data is recorded.

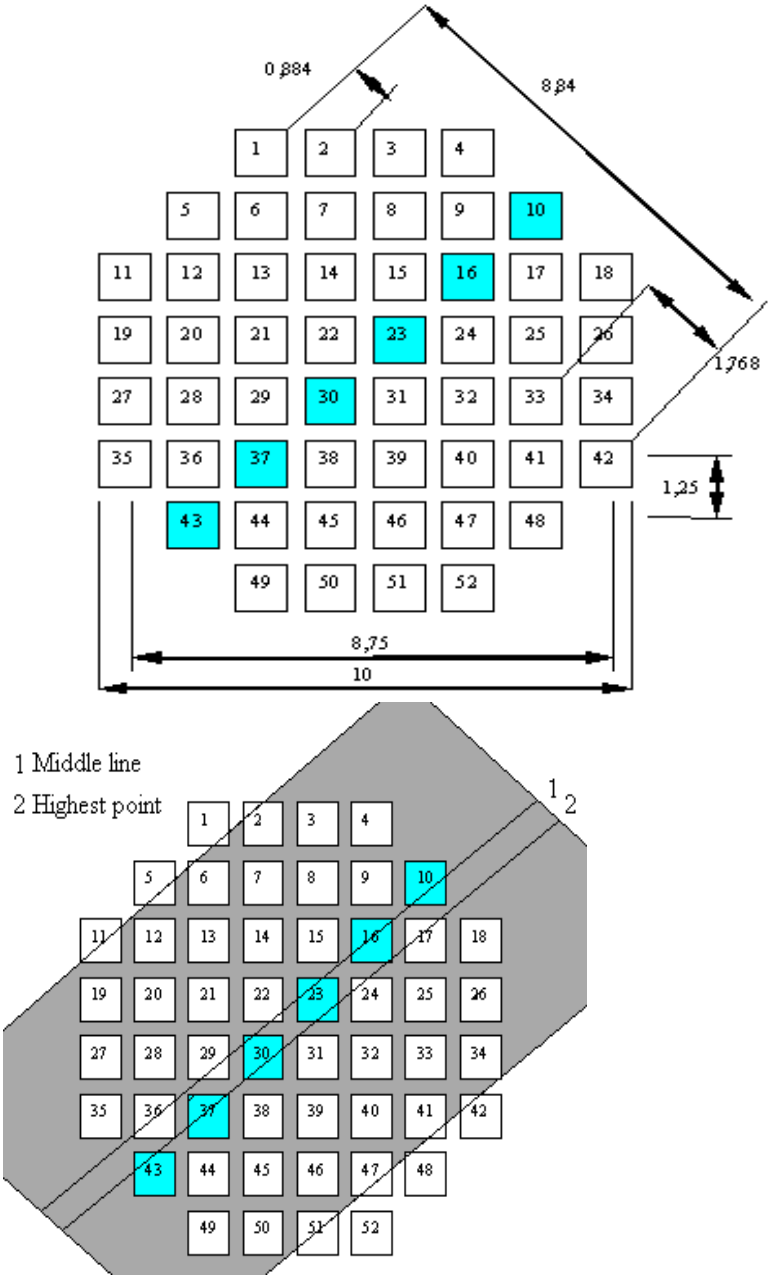

Figure 6.1 a (top) Layout of transducer channels (distances in mm), b (bottom) applied coating and regions of interest.

Before progressing any further there is a very important issue to discuss and that is the subject of heating effects. It is well documented that sound velocity is dependent on the temperature of the material and with GDS; the impacting particles will cause the substrate temperature to increase. Despite this, the current online monitoring method does not account for temperature. However, this may not be as large a concern as it first may seem. As will be seen, the time delay that is being studied is actually between the top of the substrate and the added coating. Therefore if the delay between the bottom and top of the substrate changes it should not have much effect on the area of interest. Secondly for LPGDS since the particles are injected in the divergent part of the nozzle they are not in the carrier gas for that long a period of time and therefore will not attain a high heat. This effect will have to be studied in detail later but for now, it is believed it should not have a large effect on the results.

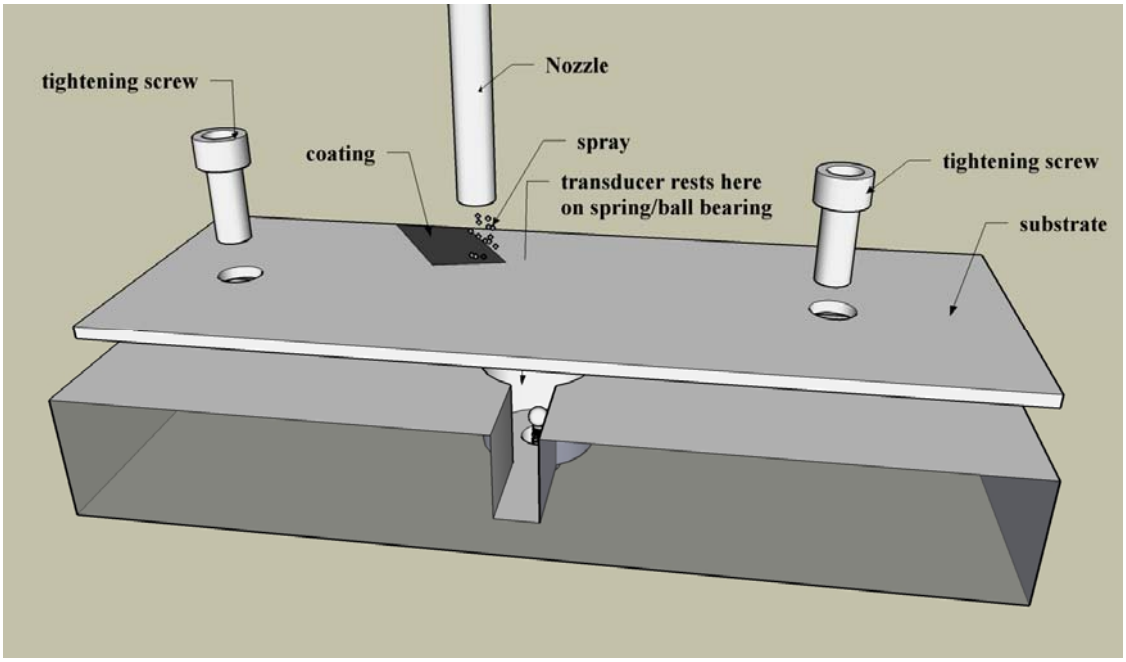

Figure 6.2 Online acoustic measurement setup.

Name	Composition	Error (mm)
1	Al+10%Al_2O_3	0.00015
2	Al+25% Al_2o_3+10%Zn	0.00013
3	Al+30%Al_2O_3	0.00014
4	Al	0.00013
9 samples	Al+25% Al_2O_3+25%Zn	0.00013
Online	Al+25% Al_2O_3+25%Zn	0.00013

Table 6.2 Error in thickness measurements for each material.

3 Error Analysis

As in previous chapters how well the peaks representing the areas of interest can be differentiated will contribute to the error. The difference is that now the measurement of interest is thickness (σ*d). Since the velocity (V) used is that calculated for the bulk material, the only error contributions will come from time (σ*t). Thus, the error measurement will be:

$$\sigma * d = V(\sigma * t) \qquad 6.1$$

One immediate consequence of this is that since the error in time is similar for all measurements, the error in thickness will be constant. Calculating these values gives the errors for each material as per table 6.2.

4 Results

Figure 6.3 shows an example of the type of data that is generated by the channels within the online measurement. It is referred to as a d-scan, which is a series of multiple b-scans

(cross sectional signals) over a period of time. The data is a gray scale image where bright pixels correspond to a high level of the signal, dark pixels correspond to negative values, and zero signal looks like gray background. The frequency with which the images are taken is controlled by the number of channels used at any time and the length of the d scans. Here channels recorded data 40 times per second (25 ms period). To understand the d-scan it is necessary to read it from top to bottom. The top line shows the reflection from the bottom of the substrate while the next line shows the reflection from the top plate (the other lines are just secondary reflections and can be ignored). It can be clearly seen by studying the second line that over time we get a second reflection which is from the build-up of the coating itself. Much of the d-scan shows time where nothing is happening (before or after spray reaches element). Figure 6.4 therefore shows the important data, that of the actual coating build-up for each of the channels considered. It shows the thickness of the coating as a function of the distance the spray nozzle has traveled. To get the acoustic thickness measurements we used the time of flight and the theoretical velocities for the fully dense composites as calculated in a previous paper [12]. In addition, each channel records thickness build-up at different distances since the spray nozzle is traveling and therefore passes across each channel at a different time. This difference in fact allows us to estimate the nozzle speed during spraying simply by comparing the time at which build-up begins for channels in a line (by choosing a line parallel to spray direction). The theoretical value we calculated was averaged to 4.2 mm/s as compared to the actual measured speed of 5 mm/s.

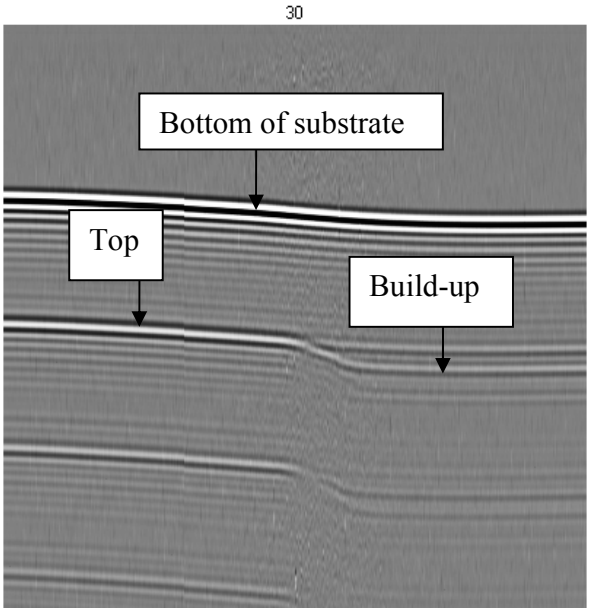

Figure 6.3 D-scan generated during online measurement.

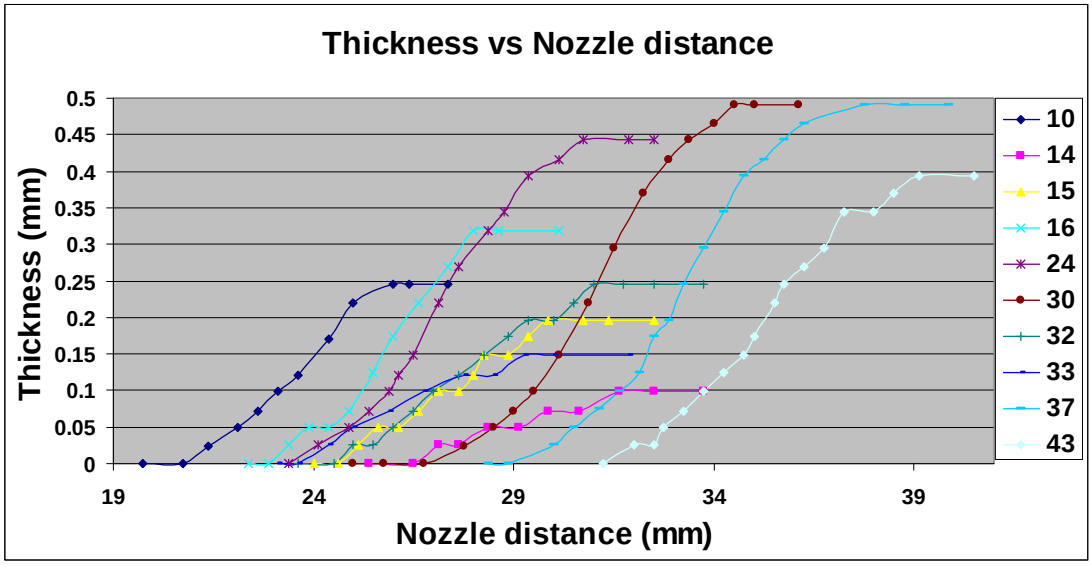

Figure 6.4 Plot of thickness against distance moved by nozzle for multiple channels.

Figure 6.5 shows the time derivative of thickness (Δthickness / Δtime) plotted against the nozzle distance for selected channels. Also shown is 2nd degree polynomial

fits to the data for each channel. This plot thus shows the rate of build-up of the coating as the nozzle moves along. It can be seen that the polynomial fit for all the channels is similar. This is true as well for the channels that were omitted (they were omitted to make the plot easier to read).

Figure 6.6 shows a cross section of the sample thickness generated from the online measurements. The position is measured as diagonal distance from the center of channel 7 (therefore measures middle point of each element). As can be seen from Figure1 plot 6 takes data from 2 lines of elements. This was done to have more data points and a more detailed cross section. The measurements on the figure show the ratio of width of spray from the left side to the peak compared to peak to right side (at the same thickness). The final plot, arguably the most important, compares the actual thickness of the samples to the thickness calculated acoustically.

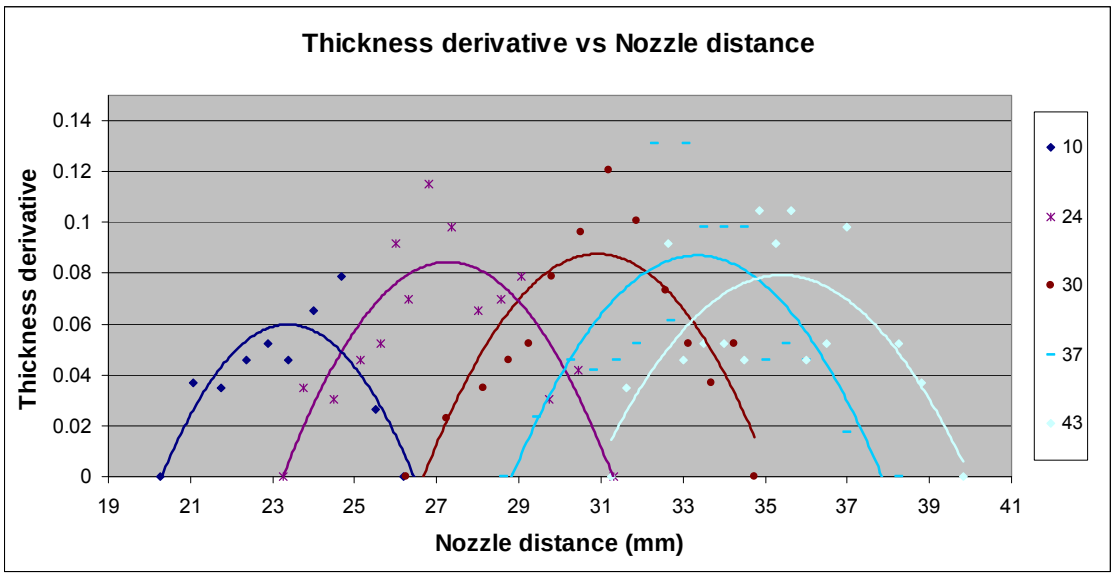

Figure 6.5 Time derivative of thickness against nozzle distance and 2nd degree polynomial fit of data.

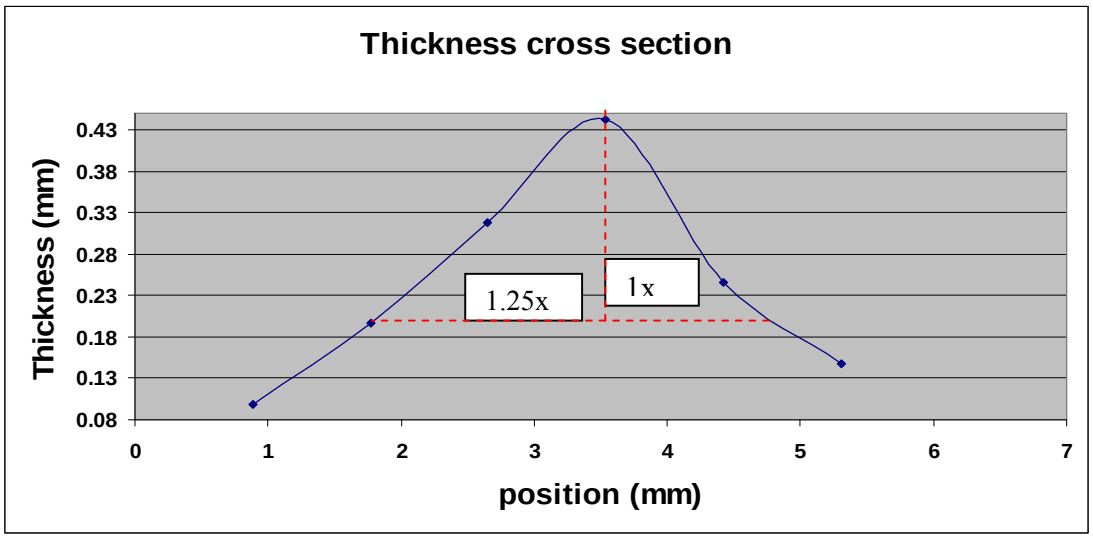

Figure 6.6 Cross section of coating thickness (channels 14, 15, 16, 24, 32, and 33 respectively).

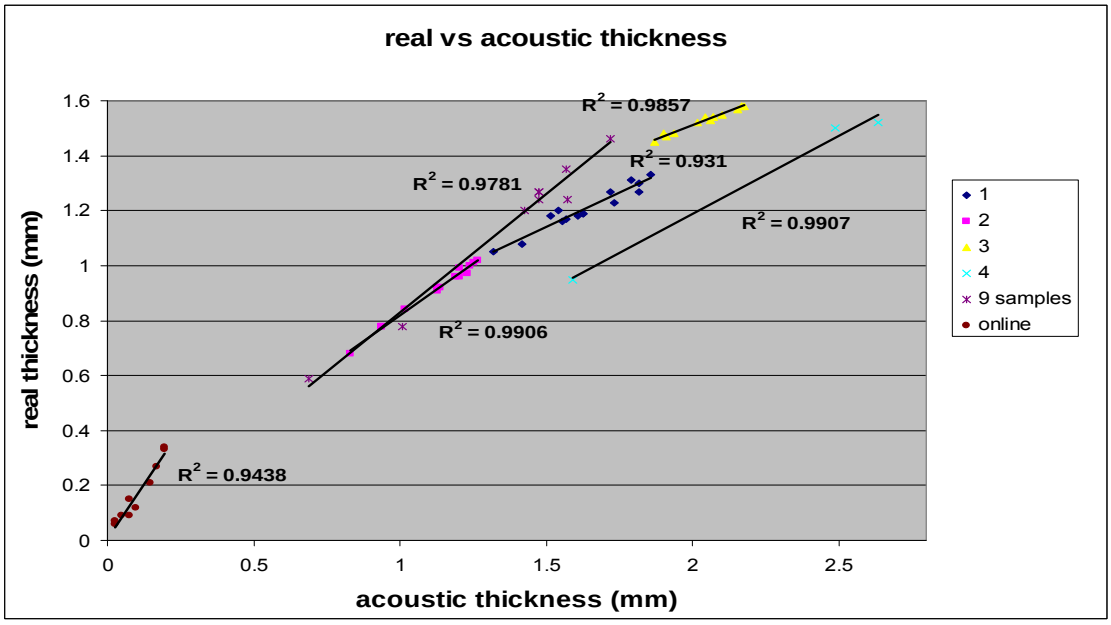

Figure 6.7 Plot of real thickness against acoustically measured thickness.

4 Discussion

Much of the results are fairly self-explanatory, but the important thing is to determine whether acoustic analysis, especially in real time is a viable method for

studying the cold spray process. Figures 6.3 and 6.4 clearly show that we can actually detect the build-up of the coating as it takes place. Not only that but we can also plot and see how it builds up over time (figure 6.5). For each channel, the 2nd degree polynomial fit gives a similar shape. It shows initially there is slow build-up, followed by a region of rapid build-up and finally it again experiences slow growth. This implies that the outer regions of the spray have less deposition take place (most likely due to lower powder concentration). These considerations can be expanded on even more through a close examination of figure 6.4. By subtracting the time at which build-up initially begins from the time at which build-up stops, we get the time for the spray to traverse across the channel. Multiplying this by the actual speed of the nozzle, than leads us to an estimate of the spray diameter. It is important to remember from figure 6.1 that the spray does not lay directly along a line of elements. Therefore, some of the elements will give a random cord of the spray diameter and underestimate. Therefore, it seems prudent to consider the channels with the largest thickness since they likely indicate the regions with the longest time and most direct spray passing over them. The channels 30 and 37 seem the most likely and they do give the highest estimates of diameter (as well as 43). The calculated value is 7-7.6 mm. This can be compared against the measured width of the coating after spraying which gave a value of 7.8 mm. This slight underestimation is most likely due to the spray not being perfectly aligned across the channels and/or the edge of the coating being to thin to give a proper reflection. Knowing that the nozzle diameter is 5 mm and the stand off distance was 15 mm it is possible to accurately describe the spray profile. It can be seen that the spray spreads out in a cone shape and thus it is very logical that the outer regions will have less powder concentration as mentioned above.

A comparison between the actual nozzle speed and that estimated acoustically seemed to give somewhat poor results. However, this can be explained quite easily due to the direction of the spray. As stated above, figure 6.1 shows the direction of spray is not perfectly along the line of transducers. This could be seen by looking at the samples themselves but also can be shown by carefully studying plot 6.4. If the spray was perfectly diagonal, than the channels in that line should all be approximately the same final height. It is clear though that channels 30 and 37 are higher and the other channels drop off (channel 23 is not shown since it had poor imaging most likely due to a lack of coupling fluid at that point) with channel 10 having the smallest thickness of all in that line. Since the actual direction of spray is different than theorized, the spray must travel a further distance from initial channel to final and therefore it is logical that we get a smaller velocity than it actually moved at.

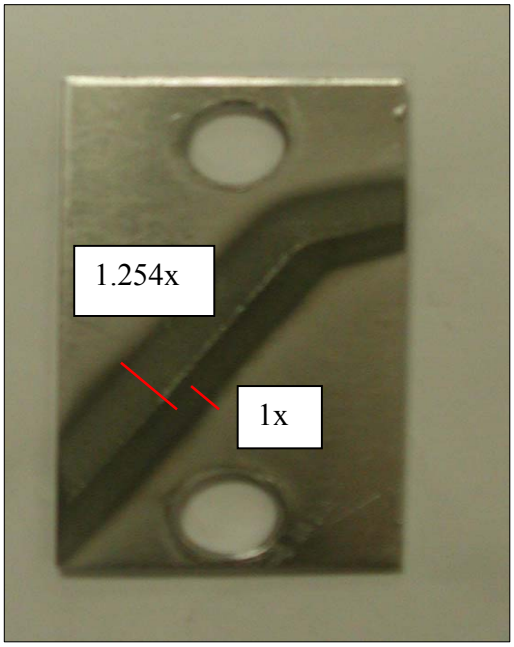

Figure 6.8 Cold sprayed sample showing ratio of dimensions.

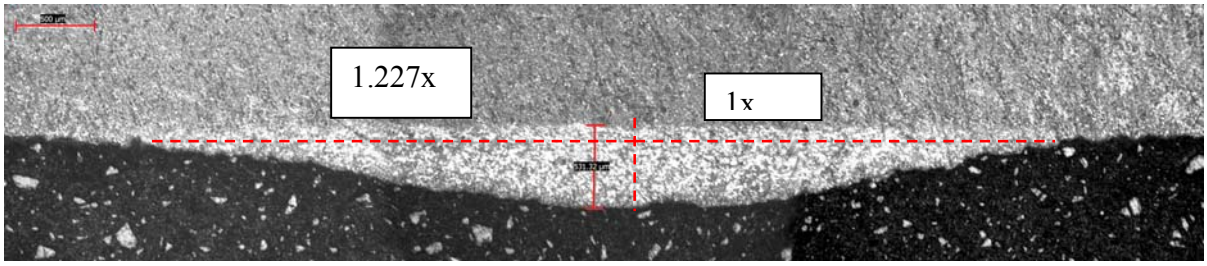

Figure 6.9 Cross section of cold sprayed sample showing dimensions.

Figure 6.6 shows a cross section of thickness for a portion of the cold sprayed samples. The profile it creates matches very well with the shape of our sprayed samples. Figure 6.9 shows a optical cross section, however we may only compare shape instead of actual thickness dimensions since it was not aligned perfectly with where the cross section was taken (would be impossible since the acoustic cross section relies on two lines of elements). Even still one can see a very odd relation that is even clearer in figure 6.8. For the cold sprayed samples created the highest point of the coating is not actually directly in the middle (the exact reason for this still needs to be explored but is likely to due with the fact that the spray is injected from one side of the gun only). In fact, by measuring it can be shown that the ratio of the left most side of the coating to the peak and that of the rightmost side to the peak is approximately 1.254:1. This agrees well with the values of 1.227:1 for the cross section. However, the most exciting aspect of this is the rough ratio predicted acoustically. In figure 6.6, it shows the measurement process. The midpoint of the two left most data points had the same thickness as the rightmost data point. Therefore, by comparing the distance from each to the center we can get an approximate ratio of left side to right side as above. The value predicted acoustically was 1.25:1. This matches up extremely well with the ratios measured in the other two methods. This shows that a very realistic cross section of the coating is created

even demonstrating the oddities of the process. While considering the ratio of left to right side makes for a nice way to compare each of the images, it is more instructional to compare to the actual ideal case expected as in figure 6.10 (not to scale). For the ideal case, the highest point is expected to occur in the middle of the sample (distance D from either side). However, in the real case the peak will occur offset to the right side. If the distances from the left and right sides to the peak are defined as A and B respectively, one can solve for the ratio of the real distances compare to the ideal case. It will be clear that for the ideal case the expected ratio will be one and if the ratio is less than one the peak is offset to that side. For simplicity, define the total width as 2.25x; this leads to the values: A = 1.25x, B = 1 x and 2D = 2.25x or D = 1.125x. Thus, the ratios obtained are:

$$\frac{A}{D} = \frac{1.25x}{1.125x} = 1.11$$

$$\frac{B}{D} = \frac{1x}{1.125x} = .89$$

this clearly shows the offset of the real values as compared to that of the ideal case. In fact, one could consider these values as the percentage of how much it is offset. It can be seen that the length A is in fact 111% the length of the ideal case while B is only 89% the ideal length (for the peak to be perfectly aligned). Thus, it can be shown that the peak is offset to the right by (11% / 2) 5.5% of the total width of the sprayed coating.

Figure 6.7 truly demonstrates the potential of acoustic analysis. For all the sets of samples there is a good fit between acoustically determined thickness and real thickness. In this case, a good fit does not necessarily mean the values are the same, but instead means a linear relationship. The actual values might be off since as said before we estimated the thickness based on the fully dense composites, which is not the case here.

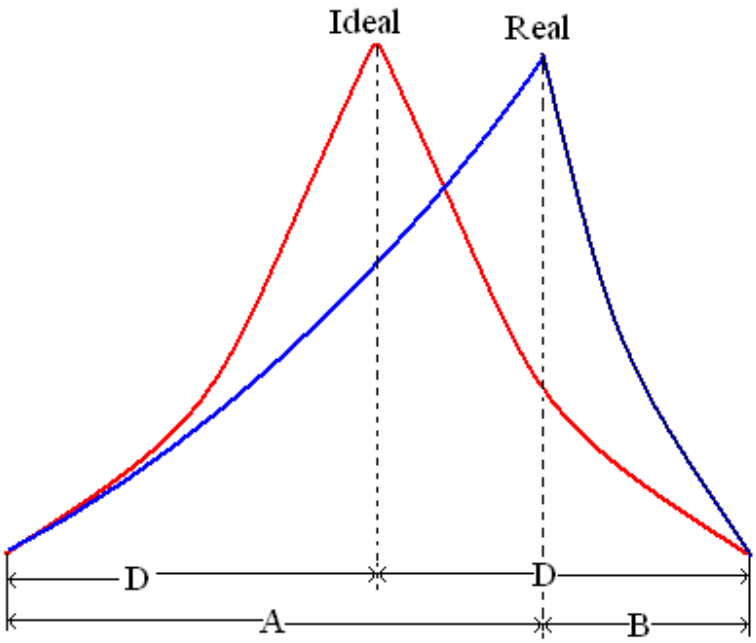

Figure 6.10 comparison of real cross section to ideal case.

This may not seem important however, we have found that the acoustic velocity for the porous cold sprayed composites is usually lower than the fully dense case (results to be published later). Thus, again the values might not be the exact same but the linear relationship for various data points shows that this is viable. Another important point to note is that many of our data sets will not have y intercepts close to 0, which you would expect since a 0 real thickness means no coating and obviously should lead to no acoustic thickness. This will obviously mean that some type of correction factor will have to be introduced to set the intercept at 0 but this is not something that has been done yet. In addition, it may not even be necessary if a database of points is made since that it will be clear that a given acoustic reading corresponds to a set real thickness. That being said, a look at the online measurements shows some very promising data. The linear fit is fairly good at about 94% but also we get a y intercept of .0072. This means the online data is

giving the closest fit to what is expected between acoustic and real thickness, in fact by introducing the point (0,0) into the data the fit is improved with R^2 = .9551, and the y intercept = .0052. Its important to be cautious however in concluding whether this is due to the measurement process or composite itself since data sets 2 and "9 samples" had similar compositions and fairly good y intercepts as well (.0767 and .0331 respectively).

5 Conclusion

The acoustic analysis showed great promise. Not only can the final value of thickness be estimated, it is also possible to see the dynamics of how the build-up takes place in real time. Figure 6.5 demonstrated that the build-up process is universal across the spray, with slower build-up at the outer extremities of the coating. Estimates of nozzle speed and spray diameter matched fairly well with the actual values and should be easy to improve by aligning the spray completely parallel to the line of channels considered. Also the cross sectional thicknesses show very accurate profiles of the actual coating structure. Most importantly, it was shown that comparing real and acoustic thickness led to a reliably linear fit for all data points. It will be important in future work to add a correction factor to zero the y intercept for aesthetics and so it fits with common logic, but it clearly is shown that thickness estimates from acoustic data is a viable method.

References

1. C. F. Rocheville, US Patent 3,100,724
2. R. C. McCune, W. T. Donlon, O. O. Popoola, and E. L. Cartwright, *Characterization of Copper Layers Produced by Cold Gas-Dynamic Spraying*, *J. Thermal Spray Technol.,* 9(1), 73-81 (2000)
3. A. P. Alkimov, V. E. Kosarev, A. N. Papyrin, Dokl. Akad. Nauk SSSr, 318, 1062-65 (1990)
4. R. C. McCune, W. T. Donlon, E. L. Cartwright, A. N. Papyrin, E. E. Rybicki, and J. R. Shadley, in: C. C. Berndt (Ed), *Thermal Spray: Practical Solutions for Engineering Problems*, ASM International, Materials Park, OH, 397-403 (1996)
5. R. B. Bhagat, M. F. Amateau, A. N. Papyrin, J. C. Conway JL, B. Stutzman JL, and B. Jones, in: C. C. Berndt(Ed), *Thermal Spray: A United Forum for Scientific and Technological Advances*, ASM International, Materials Park, OH, 361-67 (1997)
6. A. N. Papyrin, A. P. Alkimov, V. E. Koserev, in E. Lugscheider, P. A. Kammer (Eds), United Thermal Spray Conference, Dusseldorf, Germany, 288-90 (1999).
7. J. Karthikeyan, C. M. Kay, J. Lindeman, R. S. Lima, C. C. Berndt, in: C. C. Berndt (Ed), *Thermal Spray: Surface Engineering via Applied Research*, ASM International, OH, 255-62 (2000)
8. T. Stoltenhoff, H. Kreye, H. J. Richter, H. Assadi, in: C. C. Berndt, K. A. Khor, E. E. Lugscheider (Eds), *Thermal Spray 2001: New Surfaces for a New Millenium*, ASM International, Materials Park, OH, 409-16 (2001)

9. J. Karthikeyan, C. M. Kay, J. Lindemann, R. S. lima, C. C. Berndt, in: C. C. Berndt, K. A. Khor, E. E. Lugscheider (Eds), *Thermal Spray 2001: New Surfaces for a New Millenium*, ASM International, OH, 383-87 (2001)

10. G. J. Yang, F. Han, C. J. Li, in: X. Huang (Ed), *Proceedings of the Fifth International Seminar and the Sixth China national Thermal Spraying Conference*, Anshan, China, 56-61 May 21-25, 2002 (in Chinese).

11. CenterLine (Windsor) Limited**,** http://www.cntrline.com, as on 16 June 2008.

12. M. Lubrick, R. Gr. Maev, V. Leshchynsky, *Development of Cold Spray Composite Coatings Non Destructive Characterization*, MS&T 2008 Pittsburgh, Pennsylvania, (CD proceeding).

Chapter 7

Final Discussion and Future Work

1 Key points

Gas dynamic spray is still evolving both in the applications sense and in the theoretical. Countless niche markets have already been found where cold spray is the best or even only method that can be used and new applications are being discovered constantly. This market will expand even more as the process is improved. These improvements will be brought about through a deeper understanding of how fundamentally this process works. While there is some current, theories it is important to expand this knowledge and even more importantly determine the key parameters that effect coating quality. Once these parameters are known it is important to find ways to monitor them to optimize the coatings obtained. These motivations led to the development of this thesis.

The first part of the work dealt with acquiring a basic understanding of the relationships that existed between ultrasonic data and the structural properties of the coating. Sound velocity and porosity readings were used in cooperation with a model meant to describe the physical structure of the bonds within the coating. The resulting measurements for the elastic modulus fit well with the theoretical model developed. This demonstrated that ultrasonic data could be used to describe physical phenomenon.

The next portion of the thesis delved deeper into the relationship between ultrasonics and the GDS process. It was necessary to determine what effect (if any) transducer types would have on the data obtained. The optimum transducer design was determined so as accurate online monitoring of the GDS process could be obtained.

The last section of the work dealt with the actual application of the newly developed online GDS monitoring system. Promising results were obtained and analyzed and even compared very well to static (scans done on pre-sprayed samples) results. It was even possible to describe and/or predict some of the physical features of the coating and spray process itself.

2 Conclusions

The goals of this work were to use ultrasonic techniques to study and characterize the gas dynamic spray process, with the final goal of creating a feasible method for online monitoring of the process. These goals appear to have been met quite sufficiently. As stated above the earlier part of the work showed the potential to develop models relating acoustic and structural properties. While more such work is necessary, it was more logical to try to build these models based on the online data. This is especially relevant since the online results seem to hold a great deal of promise. The fit between acoustic and actual thickness measurements was 94% and had a near 0 y intercept as logic dictates it should. It was possible to get numerical estimations of both nozzle speed and spray diameter directly from the online results. Even the more qualitative d scan showed the promise of this type of test by clearly showing the build-up of the coating over time. Further analysis of that data even showed the dynamics of the build up process. Possibly most impressive of all was how accurate the acoustically created profile was to that of the physical profile. It even showed the peculiarities inherent within the process (each side of the peak not being equal). Based on this work it is already possible to use the online

monitoring system for basic estimates of coating thickness with more work the potential could be limitless. This brings us to the final section.

3 Future work

While it may seem unusual to say, this is arguably one of the most important sections of the thesis. This work was meant to be complete and able to stand upon itself however, the true benefit of this work will only be realized if it is continued. This work developed the technique through which online monitoring of the GDS process can be done, however it is now necessary to develop the theoretical considerations to go with it (work this author hopes to continue to do in a PhD). While some details are left out for obvious confidentiality reasons future work that needs to be done is discussed in general terms below.

One obvious place to start is in a discussion of the hardware itself. The current set up is not only practical but also actually the ideal setup for the current type of research. With the transducer stationary, it is possible to study the coating process at all moments (before, beginning, during, ending, and after the process takes place). Eventually however, it will become necessary to create a transducer that can travel with the spray to characterize it at all times. The current setup will not work well for this due to the need to maintain the glycerol-coupling layer between transducer and substrate. While this work is not yet necessary, ideas involving other coupling fluids/methods are already in development.

Theoretical work is by far the largest section that needs continued development. Similarly, to the earlier chapters it is necessary to study the acoustic data and develop

models relating to structural properties within the coating. This kind of analysis should be just as possible for the online measurements as the static ones. This type of analysis will allow for the non-destructive testing and estimation of properties of the coating immediately after spraying. The number of properties that would be beneficial to be able to non-destructively test are countless however, there are many key properties important to industry. Some of the most important properties to study and for which to attempt to create relations are: porosity, coating adhesion strength, coating shear strength, coating hardness, and numerous corrosion properties. Along with this, it will be necessary to study more acoustic properties such as: velocity values, acoustic impedance, reflection coefficients, etc.

Another point that needs to be studied further is the somewhat qualitative images that can be obtained. These images and the data that created them needed to be studied in more depth since they may contain more information than initially evident. As an example, consider figure 7.1. This is the same as figure 3.7 for simplicity. While it obviously shows the profile of each hole in the substrate, there also seems to be many unexplained portions. Earlier it was said that the lighter regions (in a C scan) are generally theorized to be areas of weaker bonding. However, is that always true? Moreover, if it is maybe there is a way to actually get numerical relations that accurately describe the difference in adhesion strength. Also on a related note look at the top of the B scan. The signal is a fair bit distorted and spread out. A more thorough study of the exact data that generated this image may show that there is hidden knowledge contained there (or perhaps nothing). This type of study should be done in partnership with tests of structural properties to determine what analysis (if any) can be made.

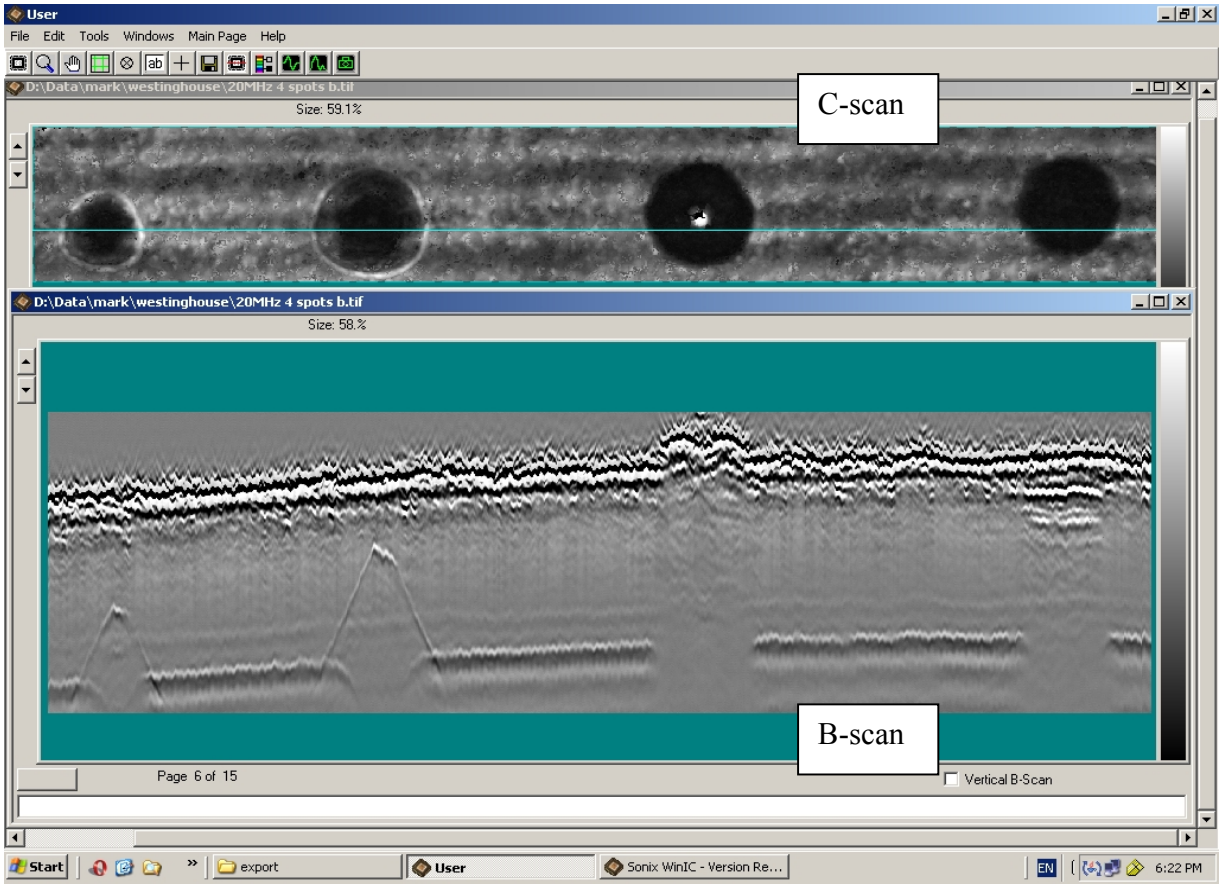

Figure 7.1 Example of C and B scans.

This brings us to the final and most ambitious work that should be undertaken. The ideal situation would be to use the online monitoring to obtain accurate data that allows for the creation of a model that describes the actual bonding of the particles during GDS. It would be necessary to consider the case of particle-to-particle bonding and that of particle to substrate bonding. This would be an extremely important piece of work since it would allow for the first conclusive description of how the process actually takes place. This deeper understanding would allow for improvements in the overall process. This and the previously mentioned work could all be coupled. With a transducer traveling with the spray and constantly generating data that may be used to estimate

properties within the coating it may even be possible to create a feed back loop so that the system monitors and optimizes itself (especially for applications with large surfaces or lots of spraying).

Full Reference List

[1] A Chertov, R Maev, F Severin, Acoustic Microscopy of Internal Structure of Resistance Spot welds, IEEE Vol. 54 No. 8 August 2007 p. 1521-1529.

[2] A. Contreras, A. Albiter, E. Bedolla, R. Perez, Advanced Engineering Materials 6, 9, (2004) 767.

[3] A. K. Mukhopadhyay, K. K. Phani, J. Mater. Sci. 33 (1998) 69.

[4] A. K. Mukhopadhyay, K. K. Phani, *J. Am. Ceram. Soc.* 20 (2000) 29.

[5] A. P. Alkimov, V. E. Kosarev, A.N. Papyrin, Dokl. Akad. Nauk SSSR 318 (1990)1062

[6] A. N. Papyrin, A. P. Alkimov, V. E. Koserev, in E. Lugscheider, P. A. Kammer (Eds), United Thermal Spray Conference, Dusseldorf, Germany, 288-90 (1999).

[7] Albert S. Birks, Robert E. Green, *Nondestructive Testing handbook,* American society for Nondestructive testing 1991.

[8] Anatolii Papyrin*, Cold Spray Technology*, Advanced Materials & Processes, 9 (2001) v159 i9 p49

[9] C. Borchers, F. Gartner, T. Stoltenhoff, H. Kreye, J. of Applied Physics 12 93(2), (2003) 10064.

[10] C. Borchers, F. Gartner, T. Stoltenhoff, H. Kreye, Acta Materialia 53, (2005) 2991.

[11] Centerline limited, http://www.supersonicspray.com/ or http://www.cntrline.com, as of Thursday December 18 2008.

[12] D. J. Green, in "An introduction to the mechanical properties of ceramics", (Cambridge University Press, 1998) p. 336.

[13] E. Maeva, A. Ackzel, Ev. Leshchinsky, Adiabatic Shear Band Formation in the Gas Dynamic Spray Process, Journal for Material Characterization, (2006) *(submitted)*.

[14] F. Tanga, H. Meeks, J. E. Spowart, T. Gnaeupel-Herold, H. Prask, I.E. Anderson, Materials Science and Engineering A 386 (2004) 194.

[15] G. J. Yang, F. Han, C. J. Li, in: X. Huang (Ed), *Proceedings of the Fifth International Seminar and the Sixth China national Thermal Spraying Conference*, Anshan, China, 56-61 May 21-25, 2002 (in Chinese).

[16] H. X. Peng, Z. Fan, J. R. G. Evans, Materials Science and Engineering A303 (2001) 37.

[17] http://www-group.slac.stanford.edu/tf/NLCTA/notes%20Fritz%20Caspers/Ultrasound.pdf as of March 25, 2009

[18] http://www.signal-processing.com/tech/us_data_liquid.htm, as of Friday December 19, 2008.

[19] http://www.inficonthinfilmdeposition.com/en/densityandacousticvalues.html, as of Friday December 19, 2008.

[20] J. Karthikeyan, International Status of Cold Spray Technology, Spraytime Vol. 12 Number 1 (2005) p1-4

[21] J. Mizusaki, S. Tsuchiya, K. Waragai, H. Tagawa, Yo. Arai, Y. Kuwayama, J. Am. Ceram. Soc.79, 1, (1996) 109.

[22] J. Karthikeyan, C. M. Kay, J. Lindeman, R. S. Lima, C. C. Berndt, in: C. C. Berndt (Ed), *Thermal Spray: Surface Engineering via Applied Research*, ASM International, OH, 255-62 (2000)

[23] J. Karthikeyan, C. M. Kay, J. Lindemann, R. S. lima, C. C. Berndt, in: C. C. Berndt, K. A. Khor, E. E. Lugscheider (Eds), *Thermal Spray 2001: New Surfaces for a New Millenium*, ASM International, OH, 383-87 (2001)

[24] J. K. Mackenzie, Proc. Phys. Soc. London, B63 (1950) 2-11.

[25] Jeganathan Karthikeyan, *Cold Spray, Advanced Materials and Processes* 3 (2005) p33-35

[26] John R. Taylor, An introduction to error analysis: the study of uncertainties in physical measurements, University Science Books; 2nd Revised edition edition.

[27] Julio Villafuerte, *Cold Spray: A New Technology*, Welding Journal 5 (2005) Vol. 84 issue 5 p24-29

[28] L. P. Martin, M. Rosin, *J. Am. Ceram. Soc* 80 (1997) 839.

[29] M. Kouzeli, A. Mortensen, Acta Materials 50, (2002) 39.

[30] M. Orrhede, R. Tolani, K. Salama, Res Nondestr Eval 8 (1996) 23.

[31] M. A. Meyers, D. J. Benson, E. A. Ollevsky, Acta mater. 47, 7, (1999) 2089.

[32] M. Lubrick, R. Gr. Maev, V. Leshchynsky, *Development of Cold Spray Composite Coatings Non Destructive Characterization*, MS&T 2008 Pittsburgh, Pennsylvania, (CD proceeding).

[33] Mark Lubrick, R. Gr. Maev, F. Severin, V. Leshchynsky, Young's Modulus of low pressure cold sprayed composites: an analysis based on a minimum contact area model, *J. Mat. Sci. (in press)*

[34] R. Prummer, Explosivverdichting Pulvriger Substanzen Grundlagen Verfahrenergebnisse (Springer, Berlin, 1987), in German.

[35] R. B. Bhagat, M. F. Amateau, A. N. Papyrin, J. C. Conway JL, B. Stutzman JL, and B. Jones, in: C. C. Berndt(Ed), *Thermal Spray: A United Forum for Scientific and Technological Advances*, ASM International, Materials Park, OH, 361-67 (1997)

[36] R. C. McCune, W. T. Donlon, O. O. Popoola, and E. L. Cartwright, *Characterization of Copper Layers Produced by Cold Gas-Dynamic Spraying*, *J. Thermal Spray Technol.,* 9(1), 73-81 (2000)

[37] R. C. McCune, W. T. Donlon, E. L. Cartwright, A. N. Papyrin, E. E. Rybicki, and J. R. Shadley, in: C. C. Berndt (Ed), *Thermal Spray: Practical Solutions for Engineering Problems*, ASM International, Materials Park, OH, 397-403 (1996)

[38] Roman Gr. Maev, Volf Leshchynsky, Introduction to Low Pressure Gas Dynamic Spray, WILEY-VCH 2008.

[39] R. Gr. Maev, Ev. Leshchinsky, in International Thermal Spray Conference Proceedings, (Seattle, USA, 2006), CD Proceeding**.**

[40] S. Klinkov, V. Kosarev, M Rein*, Cold spray deposition: Significance of particle impact phenomena*, Aerospace Science and Technology 9 (2005) p582–591

[41] T. H. Van Steenkiste, J. R. Smith, R. E. Teets, Surface and Coatings Technology 154 , (2002) 237.

[42] T. Stoltenhoff, H. Kreye, H. J.Richter, H. Assadi, in: C. C. Berndt, K. A. Khor, E. E. Lugscheider (Eds), *Thermal Spray 2001: New Surfaces for a New Millenium*, ASM International, Materials Park, OH, 409-16 (2001)

Vita Auctoris

Mark Lubrick was born in 1985 in Brampton, Ontario. In 2006, he obtained his bachelors degree in physics from the University of Windsor. He is currently a candidate for the Master's degree in Physics at the University of Windsor and hopes to graduate in winter of 2009.